

Genome-wide CRISPR screen identified a role for commander complex mediated ITGB1 recycling in basal insulin secretion



Liu Yang^{1,2}, Margret A. Fye³, Bingyuan Yang², Zihan Tang², Yue Zhang², Sander Haigh², Brittney A. Covington², Kai Bracey³, Justin W. Taraska⁴, Irina Kaverina³, Shen Qu^{1,**}, Wenbiao Chen^{2,*}

ABSTRACT

Objectives: Pancreatic beta cells secrete insulin postprandially and during fasting to maintain glucose homeostasis. Although glucose-stimulated insulin secretion (GSIS) has been extensively studied, much less is known about basal insulin secretion. Here, we performed a genome-wide CRISPR/Cas9 knockout screen to identify novel regulators of insulin secretion.

Methods: To identify genes that cell autonomously regulate insulin secretion, we engineered a Cas9-expressing MIN6 subclone that permits irreversible fluorescence labeling of exocytic insulin granules. Using a fluorescence-activated cell sorting assay of exocytosis in low glucose and high glucose conditions in individual cells, we performed a genome-wide CRISPR/Cas9 knockout screen.

Results: We identified several members of the COMMD family, a conserved family of proteins with central roles in intracellular membrane trafficking, as positive regulators of basal insulin secretion, but not GSIS. Mechanistically, we show that the Commander complex promotes insulin granules docking in basal state. This is mediated, at least in part, by its function in ITGB1 recycling. Defective ITGB1 recycling reduces its membrane distribution, the number of focal adhesions and cortical ELKS-containing complexes.

Conclusions: We demonstrated a previously unknown function of the Commander complex in basal insulin secretion. We showed that by ITGB1 recycling, Commander complex increases cortical adhesions, which enhances the assembly of the ELKS-containing complexes. The resulting increase in the number of insulin granules near the plasma membrane strengthens basal insulin secretion.

© 2022 The Author(s). Published by Elsevier GmbH. This is an open access article under the CC BY license (<http://creativecommons.org/licenses/by/4.0/>).

Keywords Commander; Integrin beta1; CRISPR screen; Insulin secretion; Endosomal recycling; Focal adhesions

1. INTRODUCTION

Insulin secreted from pancreatic beta cells is used to stimulate glucose uptake for cellular fuel and storage. Insulin secretion is continuous but peaks soon after meals, upon glucose stimulation [1]. Glucose is the most potent stimulus of insulin secretion. Inappropriate responses to glucose by beta cells can cause hypoglycemia and hyperglycemia, with the latter representing a hallmark of diabetes. Much has been learned about glucose-stimulated insulin secretion (GSIS) in the past 6 decades [2]. However, much is still unknown about insulin secretion, particularly during fasting [3].

A prerequisite for insulin secretion is the biogenesis of insulin granules and their trafficking to the plasma membrane [4]. Insulin granules, both newly formed in the Golgi complex and recycled from endosomes, migrate along cytoskeletal tracks to the plasma membrane. The cortical microtubule stabilizing center (CMSC) that anchors microtubules is critical for the delivery of insulin granules to the proximity of

the plasma membrane [5]. Upon arrival, insulin granules dock on the plasma membrane by the clustering syntaxin1 and Munc18-1 family [6]. Docking is critical for granules to be secreted following priming and a rise of intracellular Ca^{2+} , which triggers the fusion of the plasma membrane and the granule membrane [7].

Identifying the mechanism of glucose-stimulated insulin secretion (GSIS) has been a major research focus [7]. Products from glucose metabolism induce insulin secretion through at least two pathways: the ATP-mediated triggering pathway and other metabolite-mediated amplifying pathway. The triggering pathway has been extensively described [7]. It consists of the ATP-sensitive K^+ channel and voltage-dependent Ca^{2+} channels. In contrast, the amplifying pathway is not well defined. Several glucose metabolites have been proposed to activate the amplifying pathway, including acetyl-CoA [8], phosphoenolpyruvate [9], NADPH [10], and adenylosuccinate [11]. However, the mechanism by which they amplify GSIS is not clear [12].

¹Department of Endocrinology and Metabolism, Shanghai Tenth People's Hospital, School of Medicine, Tongji University, Shanghai 200072, China ²Department of Molecular Physiology and Biophysics, Vanderbilt University School of Medicine, Nashville, TN 37232, USA ³Department of Cell and Developmental Biology, Vanderbilt University School of Medicine, Nashville, TN 37232, USA ⁴Biochemistry and Biophysics Center, NHLBI, NIH, Bethesda, MD 20892, USA

*Corresponding author. E-mail: wenbiao.chen@vanderbilt.edu (W. Chen).

**Corresponding author. E-mail: qushencn@hotmail.com (S. Qu).

Received April 25, 2022 • Revision received June 30, 2022 • Accepted July 1, 2022 • Available online 11 July 2022

<https://doi.org/10.1016/j.molmet.2022.101541>

Half of the daily insulin secreted is released during fasting when blood glucose is at basal levels. Basal insulin is important for maintaining fasting blood glucose by inhibiting hepatic gluconeogenesis and glycogenolysis. Regulation of basal insulin secretion is not well studied compared to GSIS [3]. Similar to asynchronous release and spontaneous release of synaptic vesicles, basal insulin secretion may involve multiple mechanisms [13]. The cellular composition of synaptotagmins (Syt) with different Ca^{2+} sensitivity can influence basal insulin secretion. For example, the high basal insulin secretion of immature beta cells is a result of higher Ca^{2+} sensitivity due to lower expression of Ca^{2+} -insensitive Syt4 [14]. However, a dynamic change of Ca^{2+} sensitivity in adult beta cells has not been reported. The number of docked insulin granules also regulate basal insulin secretion. For example, loss of Rim2 α , a protein important for insulin granule docking, leads to lower basal insulin secretion [15]. Other mechanisms that regulate basal insulin secretion remain to be discovered.

Integrin β 1 (ITGB1) plays an important role in beta cell development and function. Constitutive loss of *Itgb1* in beta cells impairs their proliferation [16], while conditional loss of *Itgb1* in beta cells impairs GSIS [17]. ITGB1 targets insulin granules to the vascular facing cell cortex through focal adhesion-mediated positioning of the presynaptic scaffold proteins ELKS and Liprin [18,19]. ELKS is a multivalent protein that can interact with multiple components of the secretory machinery, including Liprin- α isoforms, RIMs, bassoon, LL5 β and voltage-dependent Ca^{2+} channels (VDCC) [20]. In pancreatic beta cells, ELKS is localized at the secretion sites of insulin granules, consistent with its scaffolding role in the secretion sites [21]. Although ELKS is important for synaptic vesicle docking in neurons [22], loss of ELKS in beta cells does not change insulin granule docking [23], possibly due to functional redundancy [22]. ELKS increases VDCC levels in vascular adjacent membrane [23]. Through its interaction with LL5 β , ELKS can direct insulin granule distribution by anchoring the cortical microtubule stabilizing complex (CMSC) to focal adhesions [5].

Genome-wide CRISPR screen is a promising approach to better understand insulin secretion [24]. The CRISPR system consists of a Cas9 protein and a guide RNA, often in the form of single guide RNA (sgRNA). Each sgRNA targets Cas9 to a specific sequence. In a genome-scale screen, a library of sgRNAs (usually consists of 100,000 sgRNAs) targeting all genes are expressed individually with Cas9 to generate a library of mutant cells. Cells with abnormalities are collected to determine the underlying causes. The sgRNAs that are enriched or depleted in these cells identify the responsible genes. For functional defects that do not change viability like GSIS, however, a high throughput method to identify individual cells with functional defects is necessary for such screens. Currently, no high-throughput single cell secretion assay in beta cells is available. The lack of such an assay for insulin secretion has prevented the application of Cas9-based screen in insulin secretion. Therefore, we developed a system for assaying single cell secretion in beta cells and performed a genome-wide CRISPR screen to identify candidate genes that, when mutated, increase or decrease the ratio of secretion at high and low glucose concentrations. We identified a role for the Commander complex in insulin granule docking and insulin secretion under basal glucose conditions. Mechanistically, the Commander complex promotes basal insulin secretion at least in part through recycling ITGB1 from Rab4-positive endosomes to the plasma membrane. Defective ITGB1 recycling decreases the number of cortical focal adhesions and the ELKS-containing complexes. Defective ITGB1 recycling also reduces the number of docked insulin granules and their secretion.

2. MATERIALS AND METHODS

2.1. Antibodies, plasmids and other reagents

Primary antibodies diluted in PBS with 1% BSA (for immunofluorescence) or 5% BSA (for immunoblotting) were Cas9 (Cell Signaling Technology, #14697), COMMD1 (Proteintech, 11938-1-AP), COMMD3 (Proteintech, 26240-1-AP), COMMD5 (Proteintech, 10393-1-AP), CCDC22 (Proteintech, 16636-1-AP), CCDC93 (Proteintech, 20861-1-AP), ITGB1 (Millipore, MAB1997), ITGAV (BD Biosciences, 550,024), Vincullin (Santa Cruz, sc-73614), Paxillin (BD Biosciences, 610,051), and ELKS (Abcam, ab50312). Phalloidin was from Invitrogen (A22287). Plasmid pLenti-Cas9-Blasticidin and plentiCRISPR-E (Addgene #78852) were gifts from Feng Zhang (MIT and Broad Institute) (Addgene #52962). EGFP tagged Canine Rab4, Rab5, Rab7, and Rab11 were gifts from Marino Zerial (Max Planck). A plasmid containing the coding sequence of SNAP-PHOGRIN-EGFP was constructed by HiFi assembly using PCR fragments. The final reporter construct was made by HiFi Assembly using PCR fragments containing SNAP-PHOGRIN-EGFP, PROINUSLIN-NanoLuc (a gift from David Altshuler, addgene #62057), and pLenti-RIP (a gift from David Jacobson, Vanderbilt). The mutant ITGB1 was made by linear amplification of pcDNA3.1-hITGB1 (a gift from Roy Zent, Vanderbilt Medical Center) using Q5[®] High-Fidelity DNA Polymerase and two primers: 5'-GGACACGGGTGAAGCTGCTATTATAAGAGTGCC-3' and 5'-TAACAAGTGTGGTCGCTCGGAAGTATGAGGGA-3'. SNAP substrates were purchased from NEB (SNAP-Surface[®] Block, S9143S; SNAP-Surface[®] Alexa Fluor[®] 546, S9132S; SNAP-Surface[®] Alexa Fluor[®] 647, S9136S).

2.2. Lentivirus production

HEK293FT cells (a gift from David Jacobson lab, Vanderbilt) were used for virus packaging. Cells were cultured in DMEM GlutaMax with 10% FBS, 100IU/mL penicillin, and 100 mg/mL streptomycin to 50–70% confluency in 100 mm dishes. The media was then switched to DMEM GlutaMax with 10% FBS for transfection. The following DNA mixture (18.65 μ g lentiviral plasmid, 13.9 μ g packaging plasmid (pCMV-dR7.74psPAX2), and 5.56 μ g envelope plasmid (pMD2. G) was used together with Takara CalPhos[™] Mammalian Transfection Kit (#631312) as instructed. Cells were incubated with the DNA mixture for 5–7 h and then the transfection media was aspirated and replaced with fresh DMEM GlutaMax with 10% FBS. Medium containing lentivirus was harvested 72 h later and frozen at -80°C . The viral medium was thawed for transduction of MIN6 cells.

2.3. Cell culture, viral transduction and selection

MIN6 cells were obtained from Addexbio and grown in AddexBio Advanced DMEM Medium(C0003-04) containing 15% FBS, 0.05 mM 2-mercaptoethanol, and penicillin (100 U/ml)/streptomycin (100 μ g/mL). Cells were cultured at 37°C with 5% CO_2 . The cells were transduced at seeding to enhance the efficiency. Polybrene (10 μ g/mL) was added with 3rd-generation lentiviruses containing the above-mentioned lentiviral plasmids. The virus was left on the cells for 24 h and then replaced with fresh media. The virus was then allowed to express for 2–3 days. After transduction, reporter expression was confirmed by equivalent EGFP expression and Cas9 expression was confirmed by western blot.

2.4. Glucose-stimulated insulin secretion assays (NanoLuc and ELISA)

The MIN6 cells were seeded in a 12-well plate to 80–90% confluency. Cells were starved for 1 h in 1 mL KRB (114 mM NaCl, 5 mM KCl, 1.2 mM MgSO_4 , 1.2 mM KH_2PO_4 , 20 mM HEPES, 2.5 mM CaCl_2 ,

25.5 mM NaHCO₃ and 0.2% BSA) containing 1 mM glucose. They were then cultured with freshly prepared KRB with 1 or 25 mM glucose for another hour. In glucose response curve experiment, cells were cultured in freshly prepared 1 mM, 5.6 mM, 11 mM and 25 mM KRB for another hour after starvation. The conditioned buffer was collected and centrifuged at 2,000 rpm for 5 min to obtain supernatants. The cells were lysed with RIPA buffer (R0278, Sigma) followed by centrifugation to obtain supernatants. The supernatants were then measured for NanoLuc using Promega Nano-Glo[®] Luciferase Assay System (Promega) or for insulin using a mouse insulin ELISA kit (Mercodia), and DNA using AccuBlue[®] dsDNA Quantitation kit (Biotium) following manufacturer's instruction. The reactions were read using a BioTek Synergy[™] H4 Hybrid Microplate Reader. NanoLuc and Insulin content was normalized to total DNA content (AccuBlue[®] dsDNA Quantitation, Biotium) in each sample. At least three independently generated sets of samples were analyzed under each condition.

2.5. SNAP staining of MIN6-6 cells in GSIS, imaging and flow cytometry analysis

MIN6-6 cells were starved for 4 h in DMEM with 10% FBS and 1 mM glucose followed by a 15-minute treatment with SNAP-Surface[®] Block (5 μM) in the same medium. After washing out the blocker, cells were sequentially treated with DMEM with 10% FBS, 1 mM glucose and 5 μM SNAP-Surface[®] Alexa Fluor[®] 546 for 20 min and DMEM with 10% FBS, 25 mM glucose and 5 μM SNAP-Surface[®] Alexa Fluor[®] 647 for another 20 min, with washes after each treatment. For imaging, cells were pre-seeded on coverslips. After staining, cells were fixed in 4% PFA, mounted on slides with AquaMount (Thermo Scientific), and imaged with Zeiss LSM880 laser scanning spectral confocal microscope (Carl Zeiss). For flow cytometry, a positive control group was treated with 40 mM KCl instead of 25 mM glucose, and a negative control group was treated with 300 μM Diazoxide in the presence of 25 mM glucose. Cells were harvested and washed before fixation in 4% PFA. Fluorescence intensity of Alexa Fluor 647 and Alexa Fluor 546 was determined using a 5-laser BD LSRII, and data were analyzed using FlowJo software (BD Biosciences).

2.6. Genome-wide CRISPR screens

Mouse CRISPR Knockout Pooled Library (Brie) [25] was purchased from Addgene. Approximately 150 million MIN6-6 cells were transduced at low multiplicity of infection (0.3–0.4). Transduced cells were selected and expanded in puromycin-supplemented media over 14 d to allow time for gene-editing and depletion of the target proteins before experiments. Two independent screens were performed. For each screen, 300 million cells were starved, blocked and sequentially stained with SNAP Alexa Fluor 546 and 647 in 1 mM and 25 mM glucose medium, respectively as described above. The cells were then washed twice in cold PBS, dissociated by 0.25% Trypsin with EDTA (Gibco), and fixed in 4% PFA-PBS for 15 min at room temperature with intermittently vortexing. Cells were then washed twice with cold PBS and resuspend in PBS +1% BSA. The cells were FACS sorted into the top 5% or bottom 5% according to their Alexa Fluor 647/Alexa Fluor 546 ratio using a 5-laser BD FACSAria III. Approximately 10 million cells were recovered for each population. Sorted cells were then pelleted by centrifugation, and the cell pellet was frozen at –80 °C before genomic DNA isolation. Approximately 80 million unsorted cells (1,000 × coverage per library element) were saved for screen data normalization. Genomic DNA was extracted using NK cell lysis buffer (50 mM Tris–HCl, 50 mM EDTA, 1% SDS, pH = 8.0) from sorted or unsorted cells, respectively. The genomic DNA were sent to CD Genomics for sequencing of sgRNAs. Readcount tables and gene

enrichment analysis were performed using the MAGeCK algorithm (<https://sourceforge.net/projects/mageck/>).

2.7. CRISPR-Cas9 genome editing of candidate genes

To edit *Commd3* and *Commd5*, two independent guide sequences were selected targeting the 5' constitutive exons of the gene. The sequence of the two *Commd3* sgRNA are: 5'-GAGAGCCGCTTACC-TAGCG-3', 5'-GTTTCGCGCTTCTCCTCCGG-3'. The sequence of the two *Commd5* sgRNA are: 5'-ATTCGACACAGAGGCAGCG-3', 5'-CGCTGCCTCGTGTGTCGAAT-3'. Oligonucleotides containing the guide sequence were cloned into the pLentiCRISPR-E vector (# 78,852; Addgene). Lentiviruses produced from the CRISPR plasmids were used to transduce MIN6 or MIN6-6 cells as mentioned above. Cells transduced with virus from empty pLentiCRISPR-E vector were used as the control. The transduced cells were consecutively selected using 1 μg/mL puromycin for 7 days (P8833; Sigma). Gene editing was confirmed by western blot.

2.8. Immunoblotting

Cells were lysed in RIPA lysis buffer (R0278, Sigma) supplemented with a protease inhibitor (30,496,700, Roche) and phosphatase inhibitor cocktail (P5726, Sigma). Lysates were boiled in 1 × sample buffer (#1610747, Bio-Rad), resolved on 4–20% Mini Protean TGX Precast Gel (#4561096, Bio-Rad), and transferred onto PVDF membranes (IPFL00010, Millipore) using a Bio-Rad Trans-Blot system. Membranes were blocked with 5% BSA in TBS with Tween-20 for 60 min at RT. Primary antibodies were diluted in blocking buffer and incubated overnight at 4 °C. HRP-conjugated secondary antibodies (Bio-Rad Laboratories or Abcam) diluted in blocking buffer at 1:2,500 were incubated for 2 h at RT and developed using ECL (WBKLS0100, Millipore). Blots were imaged using an ChemiDoc MP Imaging System (Bio-rad) and quantified using ImageJ software.

2.9. Real-time qPCR

Commd3 knock down and control cells were washed two times with cold PBS prior to lysis by TRIZOL reagent. RNA was isolated using Direct-Zol columns and concentrated using RNA Clean and Concentrator-25 columns. Two (2) μg of isolated RNA was reverse transcribed using oligo-dT and MMLV reverse transcriptase. The cDNAs were subjected to PCR on a BioRad CFX96 machine and amplicons were detected using SYBR green. Specific SNX14 primers and HPRT1 primers (reference gene) were used (see Table S1). PCRs were run in a LightCycler 96 Real-Time PCR system (Roche). All the qPCR primers used in this study are listed in Table S1.

2.10. FluoZin-3 assay

FluoZin-3 assay was performed 2 days after seeding parental MIN6 cells and MIN6-6 cells (50:1) at <5% confluency. These MIN6-6 cells allow for more accurate determination of focal plane and TIRF angle for the assay. Cells were incubated at 37 °C in low glucose (5.6 mM glucose) KRB (114 mM NaCl, 5 mM KCl, 1.2 mM MgSO₄, 1.2 mM KH₂PO₄, 20 mM HEPES, 2.5 mM CaCl₂, 25.5 mM NaHCO₃ and 0.2% BSA) for 1.5–2 h with a change of buffer after 1 h. Cell-impermeant FluoZin-3 dye (Thermo Fisher Scientific, Cat#: F24194) in KRB buffer was added to a final concentration of 20 μM. Glucose was added together with the dye to a final concentration of 5.6 mM or 25 mM. Focal plane and TIRF angle were refined after dye addition and the recording (60 ms exposure, no delay) started within 2 min after addition of the dye for 10 min. The videos were processed by subtracting each frame from the previous frame. Every five subtracted images were grouped as a max projection through time using the

Grouped Z-project function in ImageJ and analyzed at 300 ms time resolution. Individual secretion events or ‘flashes’ were identified using ImageJ software [26] using the point tool. FluoZin-3 movies were blinded then analyzed manually. Cell borders were identified by ROI based on DIC images. Cell number and secretion events within each identified cell were calculated in ImageJ. The detailed protocol has been published previously [27].

Supplementary video related to this article can be found at <https://doi.org/10.1016/j.molmet.2022.101541>

2.11. Immunofluorescence staining

Cultured MIN6 cells on coverslips were treated with experimental conditions for 24 h. The cells were rinsed with ice-cold PBS and fixed with 4% PFA for 10 min at room temperature followed by permeabilization in 0.3% Triton X-100. The cells were then incubated with ITGB1 antibody (1:200), ITGAV antibody (1:200), vinculin antibody (1:200), paxillin antibody (1:200) and ELKS antibody (1:200) overnight at 4 °C. The cells were subsequently washed with cold PBS three times for 10 min each and incubated with Alexa Fluor 488 or 568-labeled anti-rabbit immunoglobulin G secondary antibody (1:250) (Invitrogen) at room temperature for 2 h. After three washes with cold PBS, cells were stained with Hoechst 33,342 (0.5 µg/mL) and 1.65 µM phalloidin-647 (Biotium). The coverslips were mounted on slides with ProLong Diamond mounting medium (Thermo Fisher Scientific).

2.12. Confocal and TIRF imaging

Images were acquired using a Zeiss LSM880 with Airyscan using a 63 × oil lens. DAPI, Alexa Fluor 488, Alexa Fluor 555, and Alexa Fluor 647 images were acquired sequentially using 405-, 488-, 561-, and 633-nm laser lines. Image quantification was performed using the ImageJ software.

For quantification of the size and number of focal adhesions and ELKS-containing complexes, cells were fixed and stained with ITGB1 antibody and a focal adhesion marker (vinculin or paxillin antibody) or ELKS antibody. Basal plane images were converted to 8-bit and grayscale. Cells were outlined and thresholded to avoid artificial over- or under-filling of areas. Average intensity of ITGB1 per cell, thresholded area per cell and outlined cell area were computed while the number of focal adhesions or ELKS-containing complexes per cell was counted manually. The size of these complexes was calculated by dividing the total thresholded area per cell by the number of the cognate complex per cell [28,29].

Two methods were used to determine the number or density of docked insulin granules. In WT and *Commd3* KD MIN6-6 cells, TIRF detectable phogrin-EGFP marked vesicles were defined as docked insulin granules. The cells were imaged using a Nikon TIRF2 System for TE2000 with a TIRF 100 × 1.49 NA oil immersion lens. The granules were counted with the ImageJ software.

To determine the number of stably docked vesicles, pCMV-NPY-EGFP transfected WT and *Commd3* KD MIN6 cells were preincubated with 5.6 mM glucose for 1h. After replacing the medium with freshly made KRB buffer containing 5.6 mM, the cells were imaged on a TIRF microscope for 5 min at 1 frame/s. The first and last 5 frames were averaged. The averaged images were compared to identify insulin granules that remained in the same vicinity. These granules were considered as stably docked.

To determine the release probability of insulin granules, pCMV-IAPP-Emerald transfected WT and *Commd3* KD MIN6 cells were preincubated in medium with 5.6 mM glucose for 1h. After replacing the medium with freshly made KRB buffer containing 5.6 mM, the cells

were imaged on a Nikon TIRF2 System for TE2000 with a TIRF 100 × 1.49 NA oil immersion lens for 10 min at 1 frame/s. A secretion event was defined as a sudden disappearance (with in 1 s) of a docked vesicle.

2.13. Statistics

Results are expressed as the mean ± SEM unless otherwise specified. For data sets where the distribution was appropriate (normal distribution as determined by the D’Agostino & Pearson omnibus normality test), statistics were calculated by one-way ANOVA with Tukey’s multiple comparisons test. When the data distribution was non-normal, a Kruskal–Wallis nonparametric and multiple comparison test was used (>2 data sets). Means were compared using Student’s t test when two experimental conditions were compared. GraphPad Prism 9 was used for statistical analyses and graphical representations. Significance was defined at $p \leq 0.05$.

3. RESULTS

3.1. Development of a MIN6 reporter cell line for bulk and single cell GSIS assay

A high throughput single cell assay of exocytosis of dense core granules (insulin granules) is essential for a genomewide CRISPR/Cas9 screen for genes that regulate GSIS. We chose to use a luminal SNAP tag in combination with membrane impermeant fluorescently labeled SNAP substrates to label exocytic Insulin granules. SNAP is a 20 kDa engineered form of the DNA repair protein O6-alkylguanine-DNA alkyltransferase that reacts specifically and rapidly with benzylguanine (BG) derivatives to form an irreversible covalent conjugation [30]. As the secretory granules fuse with the plasma membrane to secrete insulin, they also expose their lumen to the extracellular environment. To anchor the SNAP tag in the lumen of Insulin granules, we inserted it into the luminal region immediately downstream of the dibasic proteolytic site of the granule-specific integral membrane protein, phogrin [31]. Although its function in insulin secretion is still not clearly defined, phogrin has been used to anchor various sensors to the lumen of secretory granules [32–34]. To easily identify cells that express SNAP-Phogrin, we also fused enhanced green fluorescent protein (EGFP) to the cytoplasmic tail of phogrin. This allows selection and visualization of cells that express SNAP-Phogrin-EGFP fusion protein.

Many beta cell clones need to be tested to identify one with appropriate glucose responsiveness. This is because most beta cell lines consist of cells with heterogenous glucose responsiveness [35,36]. To facilitate clone selection, we also linked the coding sequence for a modified preproinsulin (unprocessed insulin) to that of SNAP-Phogrin-EGFP with a viral 2A sequence. The viral 2A peptide causes ribosome skipping, allowing production of multiple independent proteins from one transcript [37]. The preproinsulin gene was modified by replacing the coding sequence for the non-functional C chain with that of NanoLuciferase (NanoLuc) [38,39], the smallest luciferase with the strongest bioluminescence. NanoLuc will be packaged together and co-secreted with insulin. Thus, nanoLuc activity in the medium, which can be easily measured with high sensitivity, is a surrogate for secreted insulin. Therefore, NanoLuc allows assaying of GSIS activity in a large number of samples [38]. The reporter gene is under the control of the rat insulin promoter (Rip) as depicted in Figure 1A and was inserted in a lentiviral vector.

We chose MIN6 cells as the target for our CRISPR screen. MIN6 cells are derived from mouse insulinoma [40]. Early passage (<40) MIN6 cells are glucose responsive and have simple culture conditions [40,41]. Early passage MIN6 cells were transduced with viral

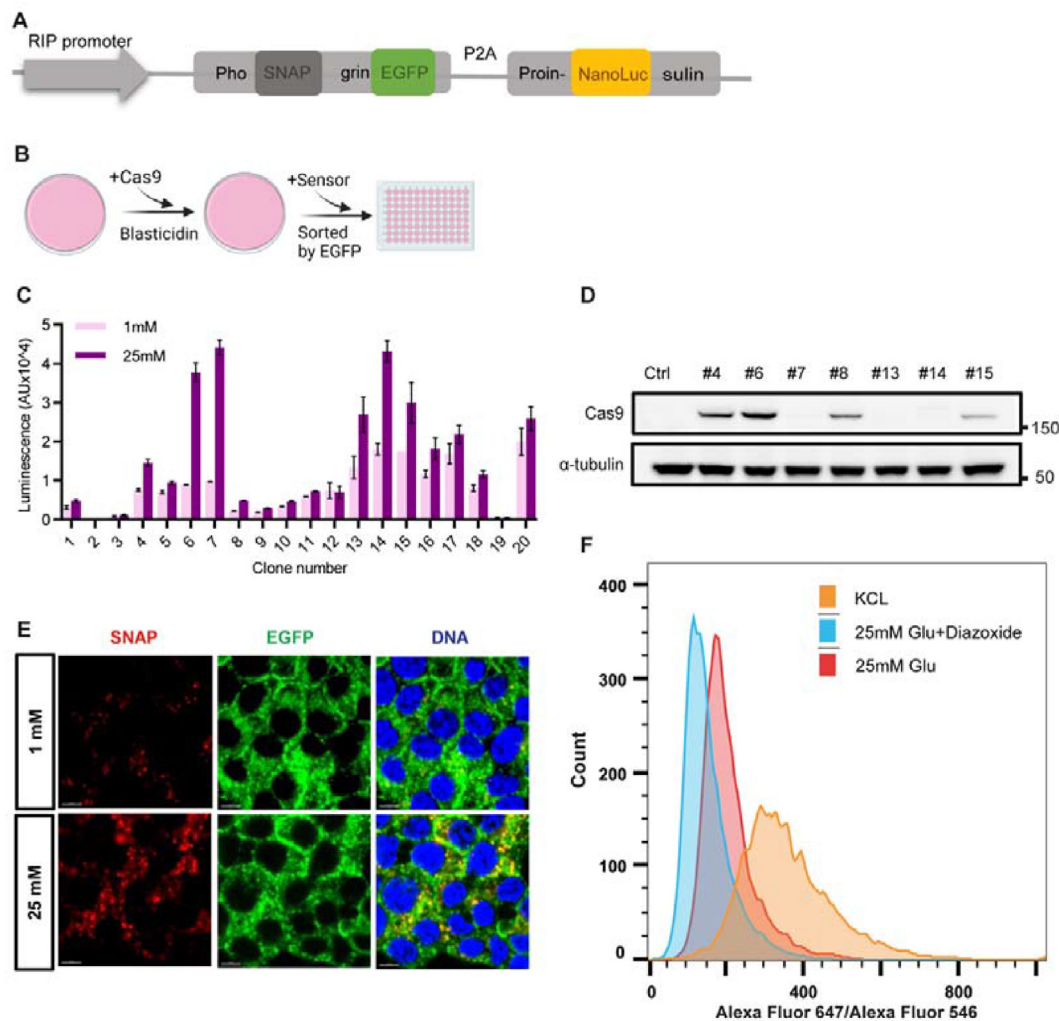


Figure 1: Development of a MIN6 reporter cell line. (A) Schematic of the reporter construct (Created with BioRender.com). (B) The workflow of establishing reporter cell clones. (C) Characterization of glucose induced insulin secretion in 20 clones. The luminescence intensity of NanoLuc was detected after 30min stimulation of 1 mM glucose (black, n = 4) or 25 mM glucose (gray, n = 4). (D) Immunoblot of Cas9 protein in control cells and clone #4, #6, #7, #8, #13, #14 and #15. (E) Representative confocal images of MIN6-6 after 20 min incubation with SNAP surface dye Alexa Fluor 546 together with 1 mM glucose or 25 mM glucose. Phogrin-EGFP was also imaged. Scale bar, 5 μ m. (F) Flow cytometry analysis of MIN6-6 cells labeled with Alexa Fluor 546 in 1 mM glucose for 20 min, followed by labeling with Alexa Fluor 647 in 25 mM glucose (red), 25 mM glucose plus 300 μ M Diazoxide (blue), or 40 mM KCl (orange).

particles of the construct and a Cas9-expressing construct, Lenti-Cas9-2A-Blast [42] (Figure 1B). After two weeks of selection, EGFP-positive cells were FACS sorted into two 96 well plates to generate clones. NanoLuc assays were performed to characterize glucose induction index of each subclone (Figure 1C, Fig. S1A). Seven subclones with a glucose induction index >2 fold were expanded and tested for the expression levels of Cas9 by western blot. The #6 subclone was chosen for additional experiments because it showed both a high GSIS index (Figure 1C) and high Cas9 expression (Figure 1D). We named this clone MIN6-6. When MIN6-6 cells were incubated sequentially in 1 mM glucose and 25 mM glucose for 30 min each, the nanoLuc activity in the latter was more than 4 fold higher, or a GSIS index >4. With a 1h incubation, the GSIS index was 10, similar to the GSIS index of 11 determined by an insulin ELISA assay (Figs. S1B–C). These results indicate that MIN6-6 is glucose responsive and the nanoLuc secretion assay is a viable surrogate for insulin secretion.

We next determined whether SNAP labeling is also glucose responsive. After queching potential surface SNAP with a non-fluorescent cell impermeant SNAP substrate, MIN6-6 cells were exposed to medium with 1 mM or 25 mM glucose containing a cell-impermeant SNAP surface dye Alexa Fluor 546. After 20 min, cells were fixed and imaged with a confocal microscope. The signal of the SNAP label was much higher in MIN6-6 cells in high glucose medium than these in low glucose medium (Figure 1E). In addition, the SNAP labels were mostly intracellular and colocalized with EGFP positive granules, probably due to compensatory endocytosis. Parental MIN6 cells without the reporter showed little SNAP labeling either in low or high glucose medium (Figs. S1C–D), indicating labeling specificity. Last, we determined whether MIN6-6 cells are compatible with the high throughput GSIS assay in single cells. After quenching, MIN6-6 cells were sequentially incubated in low glucose medium with SNAP surface dye Alexa Fluor 546 then in experimental media with SNAP surface dye Alexa Fluor 647 for 20 min each before being fixed. The

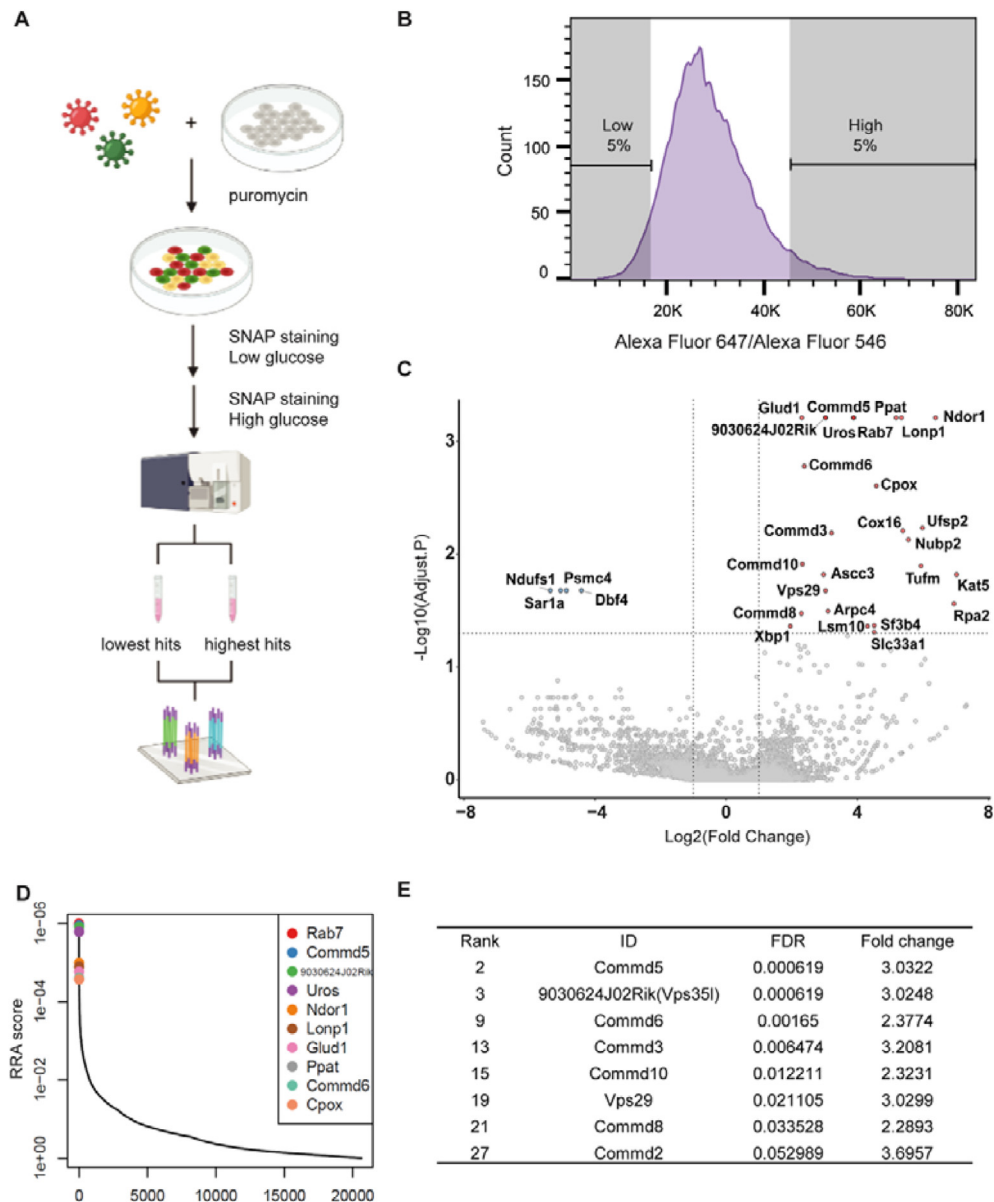


Figure 2: A genome-wide screen identifies regulators of GSIS. (A) The workflow of the screen. A genome-wide CRISPR sgRNA lentiviral library (78,637 gRNAs) was used to infect Cas9-expressing MIN6-6 cells at low MOI (0.3–0.4). After selection, most cells should express only one sgRNA. CRISPR/Cas9-edited cells were sequentially labeled with Alexa Fluor 546 in 1 mM glucose and Alexa Fluor 647 in 25 mM glucose. They were then subjected to FACS. Sorted cells were lysed for genomic DNA extraction, sgRNA amplification and next generation sequencing. (B) Top and bottom 5% cells were sorted as high and low glucose induction index according to their Alexa Fluor 546/Alexa Fluor 647 ratio. (C) A volcano plot demonstrating the FDR and fold change-based ranking of genes identified in the cells with high glucose induction index. (D) Candidate gene ranking by robust rank aggregation (RRA) scores calculated by MAGeCK. A smaller RRA score indicates more essentiality. Commander complex members and genes known to regulation insulin secretion are highlighted. (E) Table listing the Commander complex members discovered in the CRISPR screen with their rank, FDR and fold change. FDR, False discovery rate.

experimental media contained either 25 mM glucose, 25 mM glucose plus 300 μM diazoxide, or 40 mM KCl. Diazoxide is an KATP channel opener that inhibits ATP-induced membrane depolarization while KCl induces maximal insulin secretion in the absence of glucose. The fixed cells were analyzed by flow cytometry. The mean fluorescence intensity (MFI) ratio of Alexa Fluor 647/546 was used to measure glucose response index. Compared to cells stimulated with 25 mM Glucose, KCl right shifted the MFI distribution while diazoxide left shifted the MFI distribution (Figure 1F). These data confirmed that SNAP labeling intensity positively correlates with insulin secretion. MIN6-6 cells are

therefore suitable for a genomewide CRISPR screen for genes affecting insulin secretion.

3.2. A genome-wide CRISPR-Cas9 screen identifies a role for the commander complex in insulin secretion

To screen for genes important for insulin secretion, we first established a MIN6-6 mutant library using the Mouse CRISPR Knockout Pooled Library (Brie), containing 78,637 gRNAs targeting 19,674 genes and 1,000 non-targeting control sgRNAs [25]. After a two-week puromycin selection, the cells were harvested. Some cells ($\sim 8 \times 10^7$) were used

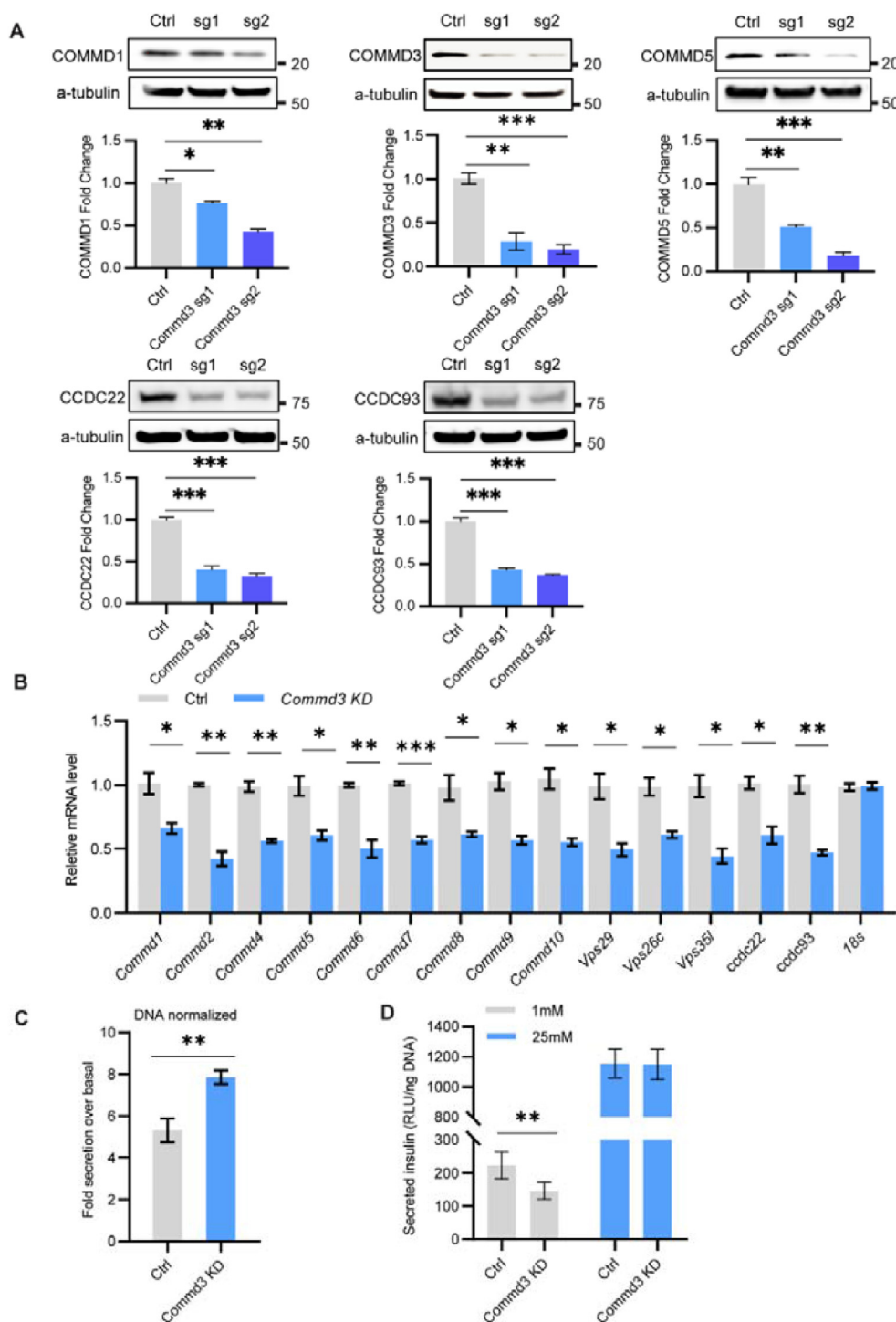


Figure 3: The Commander complex enhances basal insulin secretion. (A) Validation of *Commd3* KD cells. Two sgRNA targeting *Commd3* genes were designed to deplete COMMD3 using CRISPR/Cas9. Western blot analysis of COMMD1, COMMD3, COMMD5, CCDC22, CCDC93 and α -Tubulin in control cells and *Commd3* KD cells (control, sg1, sg2). Quantification of band intensity of each protein relative to α -tubulin. Error bar, S.E.M. (B) Quantitative RT-PCR analysis of mRNA levels of Commander complex family members in control and *Commd3* KD cells from two independent experiments. (C) Glucose induction index of control and *Commd3* KD MIN6-6 cells. (D) Basal (1 mM glucose) and stimulated (25 mM glucose) insulin secretion (using nanoLuc as a surrogate) in control and *Commd3* KD cells. Mann–Whitney nonparametric comparison *** $P < 0.001$, ** $P < 0.01$, * $P < 0.05$.

for genomic DNA to determine the sgRNA distribution, while some were used in two independent screens to identify regulators of insulin secretion. For the screen, the cells were cultured in 1 mM glucose

DMEM for 4h, followed by a 20 min incubation with SNAP-Surface Block. They were then sequentially labeled with SNAP Surface Alexa Fluor 546 in 1 mM glucose DMEM for 20 min, followed by SNAP

Surface Alexa Fluor 647 in 25 mM glucose DMEM for another 20 min. Cells were dissociated and fixed for fluorescence-activated cell sorting (FACS). Cells displaying the highest or lowest 5% Alexa Fluor 647/546 MFI ratio were collected (Figure 2A–B). The genomic DNA from these cells was isolated and the sgRNA representation was quantified by deep sequencing. Quality control showed >88% sgRNAs were present. Gini index showed an even distribution in the control sgRNA library. In the selected pools, higher cell numbers resulted in a more even distribution (Figs. S2A–C). The abundance of many sgRNAs were substantially increased in both replicates compared with unsorted control population. Nontargeting control sgRNAs exhibited no enrichment (Figure 2C), confirming that the screens were effective and specific. Genes were ranked based on the enrichment of their targeting sgRNAs using the MAGeCK (model-based analysis of genome-wide CRISPR-Cas9 knockout) algorithm [43]. The sgRNA of a few dozens of genes were enriched in the pool with increased glucose stimulation index. Some were known negative GSIS regulators such as *Glud1* and *Rab7*. However, only a few genes whose sgRNAs were enriched in the pool with decreased glucose stimulation index (Fig. S2D). The small number of hits may be due to the highly stringent cell selection. We focused on gene hits in the pool of high glucose stimulation index because these may be drug targets. Several of these genes encode enzymes catalyzing lipid or carbohydrate metabolism, mediators of gene expression, proteins important for vesicular trafficking, as well as genes lacking annotated functions. Several members of Commander complex were among the top gene hits. These include COMM Domain Containing 5 (COMMD5), VPS35 Endosomal Protein Sorting Factor Like (VPS35L), COMM Domain Containing 6 (COMMD6), COMM Domain Containing 3 (COMMD3), COMM Domain Containing 10 (COMMD10), VPS29 Retromer Complex Component (VPS29), COMM Domain Containing 8 (COMMD8), and COMM Domain Containing 2 (COMMD2) (Figure 2D–E). The identification of multiple components of the Commander complex provides strong support for its role in insulin secretion.

3.3. Loss of *Commd3* decreases basal insulin secretion

The Commander complex is important for endosomal recycling of a subset of proteins. It comprises 15 different proteins, including COMMD 1–10, CCDC93, CCDC22, VPS35L, VPS26C, and VPS29. COMMD 1–10 are thought to always exist in a complex, and loss of one lowers the expression of the rest [44]. Mutations in *Commd* genes are linked to human RS/3C syndrome, a developmental disease in humans [45]. *Commd4* and *Commd7* have been implicated in T2D in two genome-wide association studies [46,47]. However, the role of Commander complex in pancreatic beta cells has not been characterized.

We first validated that loss of the Commander complex in beta cells improves glucose stimulation index. We generated two *Commd3* KD populations in MIN6 and MIN6-6 cells using CRISPR/Cas9 with two different sgRNAs. Western blot analysis indicated that COMMD3 protein levels were decreased in both populations, with sgRNA2 population having 80–90% reduction (Figure 3B). In addition, 4 other Commander complex components, COMMD1, COMMD5, CCDC22, and CCDC93 were also reduced by 60–85% in the sgRNA2 population (Figure 3A), consistent with previous studies [48,49]. These cells are referred to as *Commd3* KD cells. Interestingly, qRT-PCR analysis of genes for the Commander complex in control and *Commd3* KD cells revealed a 40–60% reduction in the *Commd3* KD cells compared to control MIN6 cells (Figure 3B). The results suggest a feedback control at the level of either transcription or mRNA stability. *Commd3* KD cells showed a high glucose stimulation index, validating the screen

(Figure 3C). Moreover, this increase of GSIS index is mainly due to a decreased basal insulin secretion but not stimulated insulin secretion (Figure 3D). The glucose response curve showed less insulin secretion at 1 mM and 5.6 mM glucose but a normal insulin secretion at 11.1 mM and 25 mM glucose, indicating COMMD3 regulates basal insulin secretion (Fig. S3A). We confirmed that this is not specific to *Commd3* KD, we also generated *Commd5* KD cells. Similar to *Commd3* KD cells, *Commd5* KD cells also have a lower glucose induction index due to lower basal insulin secretion (Figs. S3C–E). To determine whether the low basal secretion is due to increased beta cell maturity, we compared the transcript levels of multiple maturation markers by qRT-PCR. No change was detected in the *Commd3* KD cells (Fig. S3B). Therefore, the Commander complex enhances basal insulin secretion without affecting beta cell maturity.

3.4. Loss of *Commd3* reduces the number of exocytic events and docked insulin granules

To understand the underlying mechanism of decreased basal insulin secretion, we used FluoZin-3 based live imaging on a total internal reflection fluorescence (TIRF) microscope [27,50] to examine insulin granule docking and secretion in control and *Commd3* KD MIN6 cells. FluoZin-3 increases fluorescence emission upon binding to Zn^{2+} , a component of insulin crystals in the insulin granules. And due to the cell impermeability of FluoZin-3, it only binds Zn^{2+} after secretin. A “flush” of fluorescence occurs with each exocytic event (Figure 4A). FluoZin-3 was added into the KRB buffer with 5.6 mM or 25 mM glucose and the cells were imaged for 10 min at a rate of 60 ms/frame. At 5.6 mM glucose, we detected insulin secretion in a lower fraction of *Commd3* KD cells (20%) than in control MIN6 cells (30%) (Figure 4B–E). In addition, there were fewer secretion events on average in active *Commd3* KD cells than in control cells (Figure 4B–D,F). At 25 mM glucose, there was no difference in either the fraction of active cells or average secretion events per cell between *Commd3* KD and control cells (Figure 4B–D). These results support that loss of *Commd3* decreases basal but not glucose-stimulated insulin secretion.

A decrease in basal insulin secretion could result from a decreased fusion probability or a reduced number of docked granules [51]. To investigate if the decreased basal secretion is due to fewer docked insulin granules in *Commd3* KD cells, we measured the number of vesicles near the basal membrane in the SNAP-phogrin-EGFP expressing MIN6-6 cells using TIRF microscopy. We found a significant reduction of the density of cortical insulin granules in *Commd3* KD MIN6-6 cells compared to the control MIN6-6 cells at 5.6 mM glucose. After 1 h of glucose stimulation, however, no difference was detected in the density of cortical insulin granules between *Commd3* KD and control MIN6-6 cells (Figure 5A–B). As vesicle docking is dynamic [52], some of the cortical insulin granules may be transiently docked, we therefore compared the number of insulin granules that remain docked for 5 min in pCMV-NPY-EGFP transfected control and *Commd3* KD MIN6 cells using TIRF microscopy. There was a significant decrease of stably docked insulin granules in *Commd3* KD cells compared to control cells (Figure 5C–D).

To determine whether a decreased release probability also contributes to the lower basal secretion, we determined the number of exocytic granules in pCMV-IAPP-Emerald transfected control and *Commd3* KD MIN6 cells. Exocytosis is indicated by a sudden increase followed by a disappearance of fluorescence (within 1 s) [53,54]. There was no significant difference between *Commd3* KD and control MIN6 cells (Figure 5E–F, Video 1). Together, these results suggest the decreased basal insulin secretion in *Commd3* KD cells is due to fewer docked insulin granules.

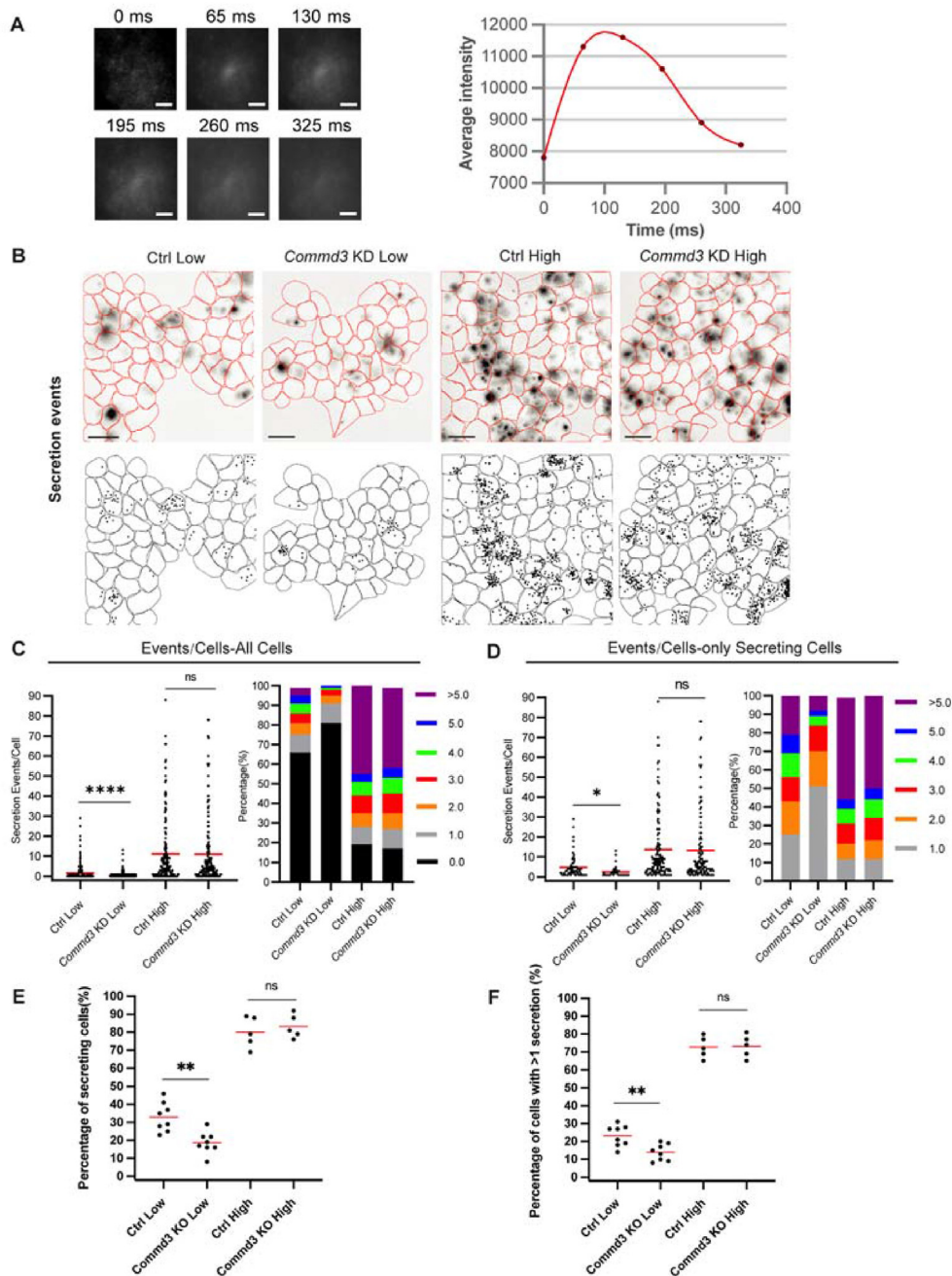


Figure 4: Loss of *Commd3* decreases the insulin secretion events at basal glucose level. (A) Representative images and average intensity of a single secretion event prior to image processing. Scale bars: 3 μ m. (B) Inverted intensity time projections of all secretion events during the duration of the FluoZin-3 assay. Upper panels. Accumulation of FluoZin-3 flashes are represented as black areas. Cell border (in red) was identified via DIC images (see Materials and methods). Lower panel. Schematic rendering of the upper panel showing cell outlines (black lines) and secretion events (black dots). Control and *Commd3* KD cells were preincubated in 5.6 mM glucose medium for 1h and followed by incubation with 5.6 mM or 25 mM glucose. Scale bars: 60 μ m. (C) Left panel, graph showing secretion events per cell at basal condition as detected by the FluoZin-3 assay. All cells in a field of view are analyzed, regardless of their activity during the assay. Red bar, mean. Kruskal–Wallis nonparametric and multiple comparison test. N = 158–200 cells from 5 to 8 dishes. Right panel, stacked histogram of the percentage of cells that had different number of secretion events. (D) Left panel, graph of secretion events in stimulated cells during the assay. Red bar, mean. Kruskal–Wallis nonparametric and multiple comparison test. N = 68–131 cells from 5 to 8 dishes. Right panel, stacked histogram of the percentage of cells that had different number of secretion events. (E) Graph of the percentage of cells with at least 1 secretion event in a field of view. Red bars, mean. One-way ANOVA and multiple comparison tests. (F) Graph of the percentage of cells with more than one secretion event in a field of view. Red bars, mean. One-way ANOVA and multiple comparison tests. ****P < 0.0001, **P < 0.01, *P < 0.05.

3.5. Loss of *Commd3* causes retention of ITGB1 in Rab4-positive recycling endosomes

Having demonstrated that *Commd3* KD decreases basal insulin secretion due to fewer docked insulin granules, we next investigated

the underlying molecular mechanism. Commander complex associates with SNX17, which mediates recycling of membrane proteins with a Φ xNPxY or Φ xNxxY sorting motif, such as ITGB1, LDLR and LRP1 [55]. *Ldlr* is expressed in MIN6 cells and is important for cholesterol uptake

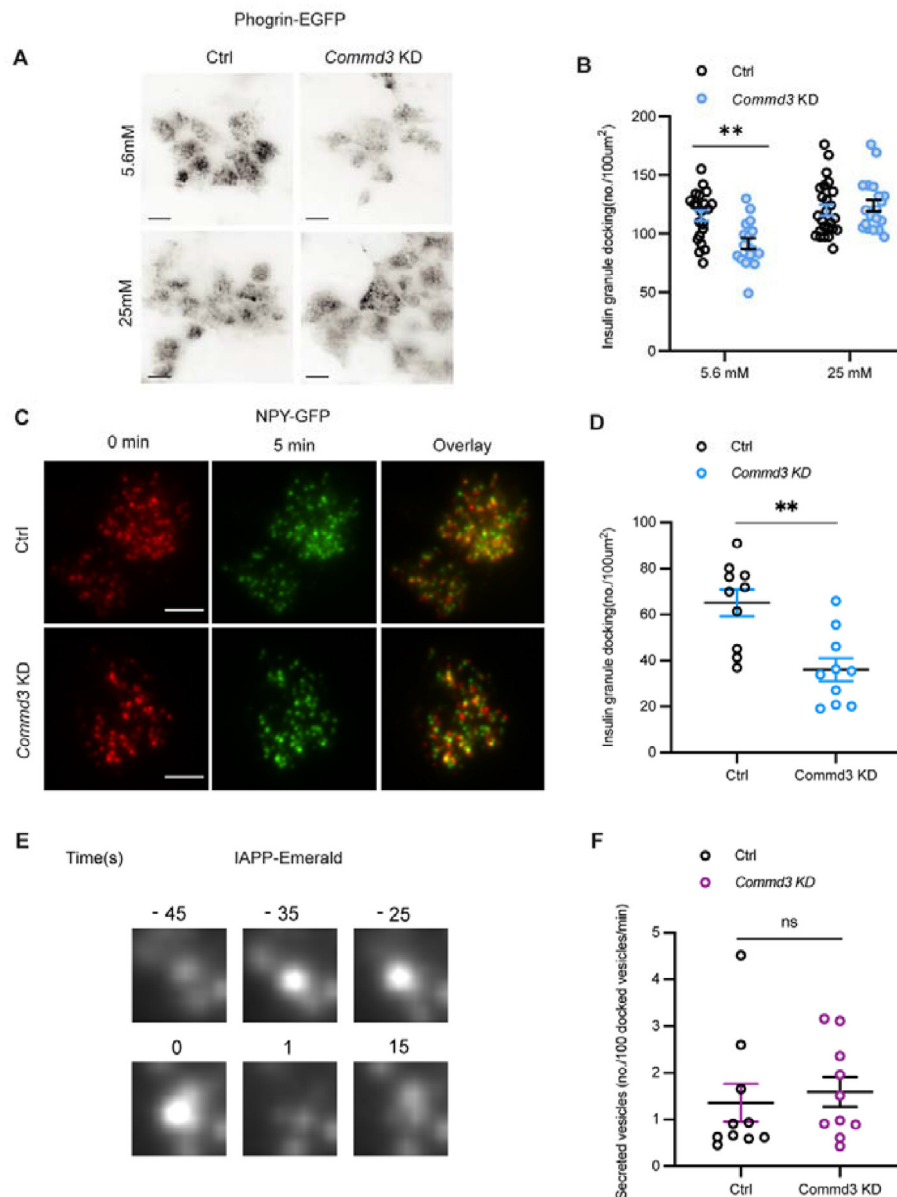


Figure 5: Loss of *Commd3* reduces docked insulin vesicles at basal glucose levels. (A) Representative TIRF images showing cortical insulin granules based on phogrin-EGFP signal. Control and *Commd3* KD MIN6-6 cells were preincubated in medium with 5.6 mM glucose for 1h followed by medium with 5.6 mM or 25 mM glucose for 1h and fixed immediately. Scale bar, 20 μm . (B) Quantification of docked insulin vesicles in control and *Commd3* KD MIN6-6 cells treated as in (A). Kruskal–Wallis nonparametric and multiple comparison test. Single data points are plotted. Horizontal line, mean; error bars, S.E.M. (C) Representative TIRF images taken 5 min apart for identification of stably docked insulin granules. NPY-EGFP transfected WT and *Commd3* KD MIN6 cells were preincubated with KRB buffer containing 5.6 mM glucose for 1h. The medium was then replaced with fresh medium. The cells were imaged on a TIRF microscope for 5 min at 1 frame/s. The first (red) and last (green) 5 frames were averaged. The two images were overlaid to identify insulin granules that remained in the same vicinity. These granules were considered as stably docked. Scale bar, 5 μm . (D) Quantification of stably docked insulin vesicles in control and *Commd3* KD MIN6 cells treated as in (C). Kruskal–Wallis nonparametric test. Single data points are plotted. Horizontal line, mean. Error bars, S.E.M. (E) Representative images showing the exocytosis of an insulin granule. IAPP-Emerald transfected WT and *Commd3* KD MIN6 cells were preincubated with KRB buffer containing 5.6 mM glucose for 1h and medium was refreshed. The cells were imaged on a TIRF microscope for 10 min at 1 frame/s. (F) Quantification of secretion events normalized to the number of stably docked granules in control and *Commd3* KD MIN6 cells treated as in (E). Kruskal–Wallis nonparametric test. Single data points are plotted. Horizontal line, mean. Error bars, S.E.M. ns, no significant difference. $**P < 0.01$. TIRFM, total internal reflection fluorescence microscope.

[56]. Cholesterol is important for the formation of Syntaxin clusters on the plasma membrane, where secretory vesicles preferentially dock [57]. Defective LDLR recycling therefore could impair insulin granules docking. However, β cell function is normal in *Ldlr* $^{-/-}$ mice [56]. Therefore, we excluded defective LDLR recycling as the mechanism for the decreased basal secretion in the *Commd3* deficient cells. Singla

et al. reported that knocking down *Commd3*, *Ccdc93*, *Vps35l* or *Vps26c* causes ITGB1 accumulation in WASH-positive intracellular vesicles in HeLa cells [48]. Mice with ITGB1 ablation in beta cells have decreased beta cell mass and impaired GSIS [16,58,59]. The role of ITGB1 recycling in insulin secretion has not been reported. Therefore, we investigated whether *Commd3* KD affects ITGB1 endocytic

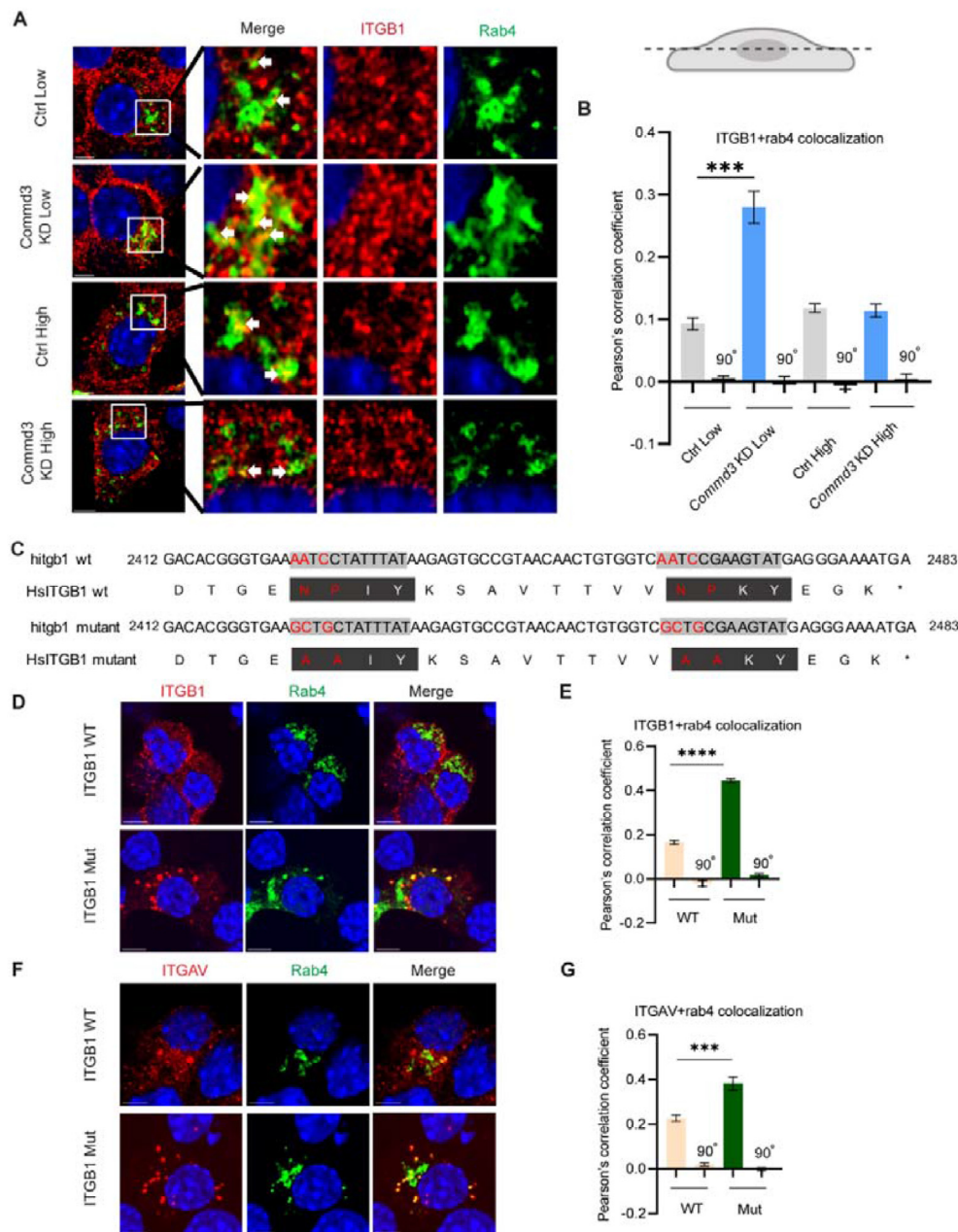


Figure 6: Loss of *Commd3* causes retention of ITGB1 in Rab4-positive recycling endosomes. (A) Representative images of ITGB1 and Rab4 subcellular localization. Control and *Commd3* KD MIN6 cells were transfected with Rab-4-EGFP, cultured in medium with 5.6 mM or 25 mM glucose, then fixed for ITGB1 immunofluorescence (red) and DNA stain (blue). The cells were imaged with a confocal microscope. White arrow, the colocalization of ITGB1 and Rab4. Scale bar, 3 μ m. (B) Quantification of colocalization of ITGB1 and Rab4 in control and *Commd3* KD MIN6 cells using Pearson's correlation coefficient between the two channels. $N = 18$ – 19 images from three independent experiments; 90° indicates a 90° rotation of one image channel to rule out nonspecific colocalization. Error bars, S.E.M. (C) Schematic showing WT and mutant ITGB1 sequences. Two NPXY motifs were mutated to AAxY. (D) Representative images of Rab4 and ITGB1 subcellular localization. Cells were treated as in (A) except that they were also transfected with WT or mutant ITGB1-expressing construct. Scale bar, 3 μ m. (E) Quantification of ITGB1-Rab4 colocalization in MIN6 cells transfected with ITGB1 WT or ITGB1 mut using Pearson's correlation coefficient between the two channels. $N = 15$ – 20 images from three independent experiments. Error bars, S.E.M. (F) Representative images of ITGAV (red) and Rab4 (green) subcellular localization in MIN6 cells transfected with WT or mutant ITGB1-expressing construct. Cells were treated as in (A). Scale bar, 3 μ m. (G) Quantification of ITGAV-Rab4 colocalization in MIN6 cells transfected with WT or mutant ITGB1-expressing construct using Pearson's correlation coefficient between the two channels. $N = 15$ – 18 images from three independent experiments. Error bars, S.E.M.

trafficking in MIN6 cells by using EGFP-tagged Rab4, 5, 7, and 11 to mark different endocytic compartments. At 5.6 mM glucose, there was extensive colocalization of ITGB1 and Rab4 in *Commd3* KD cells, in contrast to the low colocalization in control MIN6 cells (Figure 6A–B),

indicating that ITGB1 proteins are stuck in the Rab4-positive early endosome or recycling endosomes. These results are consistent with a recycling defect in ITGB1 trafficking. At 25 mM glucose, however, the colocalization of ITGB1 and Rab4 was low in both *Commd3* KD cells

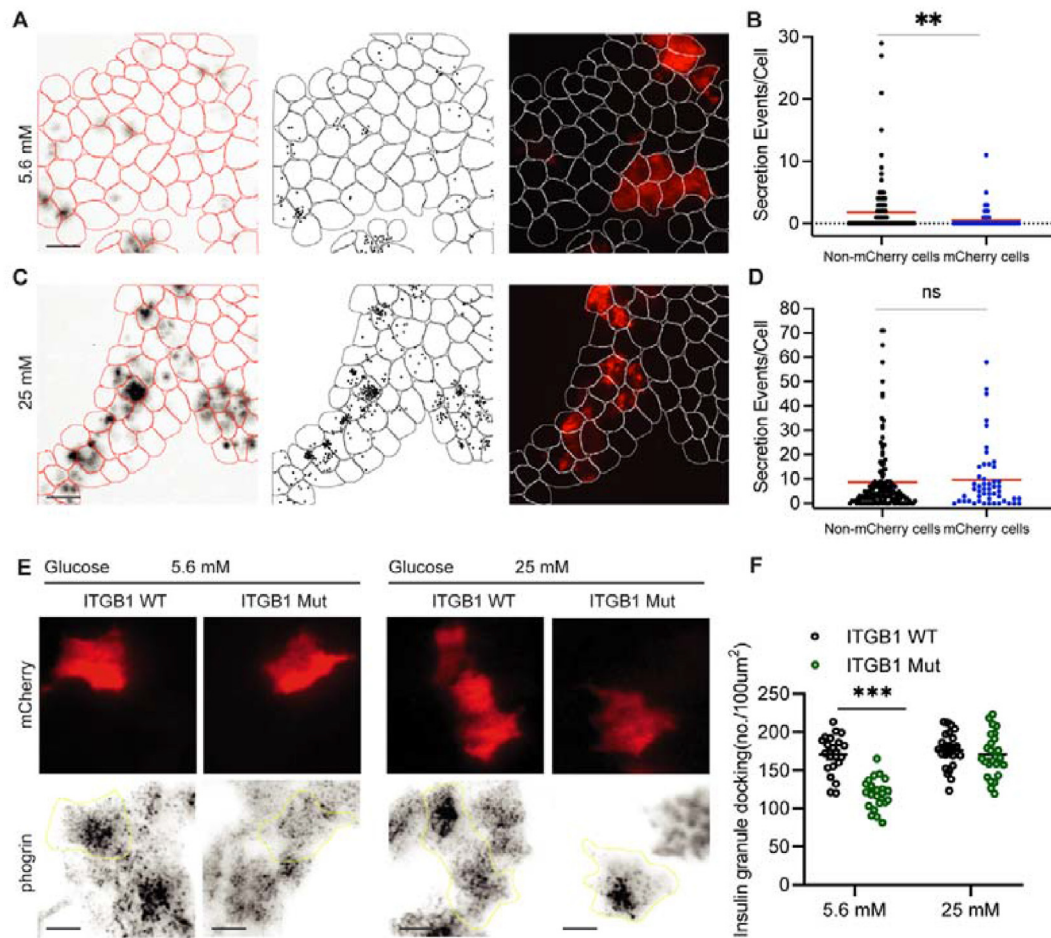


Figure 7: Defective ITGB1 recycling impairs insulin granule docking and basal insulin secretion. (A) Insulin secretion events detected by FluoZin-3 in MIN6 cells co-expressing mCherry and mutant ITGB1 and their untransfected neighbors. After transfection, the cells were preincubated in 5.6 mM glucose medium for 1h followed by fresh medium with 5.6 mM mCherry indicates transfected cells. Scale bars, 60 μ m. (B) Quantification of secretion events per cell detected by FluoZin-3 assay at 5.6 mM glucose. All cells in a field of view were analyzed regardless of transfection status. Red bar, mean. Kruskal–Wallis nonparametric and multiple comparison test. N = 75 mCherry -cells and 200 non-mCherry cells from 5 to 10 dishes. (C) Representative images showing insulin secretion detected by FluoZin-3 in MIN6 cells expressing co-expressing mCherry and mutant ITGB1. MIN6 cells expressing exogenous WT or mutant ITGB1 were preincubated in 5.6 mM glucose medium for 1h followed by fresh medium with 25 mM glucose. mCherry-cells indicated transfected cells. Scale bars: 60 μ m. (D) Quantification of secretion events per cell detected by FluoZin-3 assay at 25 mM glucose. N = 50 mCherry-cells and 150 non-mCherry cells from 5 to 10 dishes. (E) Docked insulin granules in MIN6-6 cells co-expressing mCherry and WT or mutant ITGB1. Top panel. Images showing mCherry transfected (red) and untransfected cells. Bottom panel. TIRF images showing insulin granules (Phogrin-EGFP positive vesicles). After transfection (48h), cells were preincubated in 5.6 mM glucose medium for 1h, stimulated with 25 mM glucose medium for 1h and fixed immediately. mCherry-cells indicated transfected cells. Scale bar, 10 μ m. (F) Quantification of docked insulin vesicles in MIN6-6 cells expressing WT or mutant ITGB1 analyzed as in (E). N = 21–25 cells. Kruskal–Wallis nonparametric and multiple comparison test. Single data points are plotted. Horizontal line, mean. Error bars, S.E.M. ns, no significant difference, ***P < 0.0001, **P < 0.01.

and control MIN6 cells, indicating the activation of a different recycling mechanism. There was no difference in ITGB1 colocalization with Rab5, Rab7 or Rab11 between *Commd3* KD cells and control cells in both basal glucose and high glucose conditions (Fig. S4).

3.6. Defective ITGB1 recycling impairs insulin granule docking and basal insulin secretion

We next investigated whether the decreased basal insulin secretion and insulin granule docking in *Commd3* KD cells is due to defective SNX17-mediated ITGB1 recycling. We mutated the Φ xNPxY motifs of human ITGB1 (Figure 6C) and performed cotransfection to co-express Rab4-EGFP with either the wild type or the mutant ITGB1 in MIN6 cells. We found that, just as in the *Commd3* KD cells, there was an increase of ITGB1 in Rab4-positive vesicles in cells expressing the mutant ITGB1

compared to those expressing the wild type ITGB1 (Figure 6D–E). As ITGB1 can dimerize with at least 12 α subunits [60], we examined whether endogenous α subunits are also retained in the Rab4-positive vesicles. Integrin AV transcript is the most abundant α integrin in MIN6 cells [61]. In MIN6 cells expressing mutant ITGB1, ITGAV was also sequestered in the Rab4-positive vesicles as expected (Figure 6F–G). To determine whether the mutant ITGB1 affects insulin secretion, we co-transfected expression vectors for mCherry and mutant ITGB1 in MIN6 cells. We then performed the FluoZin-3 assay to quantify the insulin secretion events under 5.6 mM and 25 mM glucose in transfected and untransfected cells. At 5.6 mM glucose, we found a much lower percentage of cells that secrete insulin compared to untransfected cells. The average secretion events in cells expressing the mutant ITGB1 were also decreased compared to untransfected cells

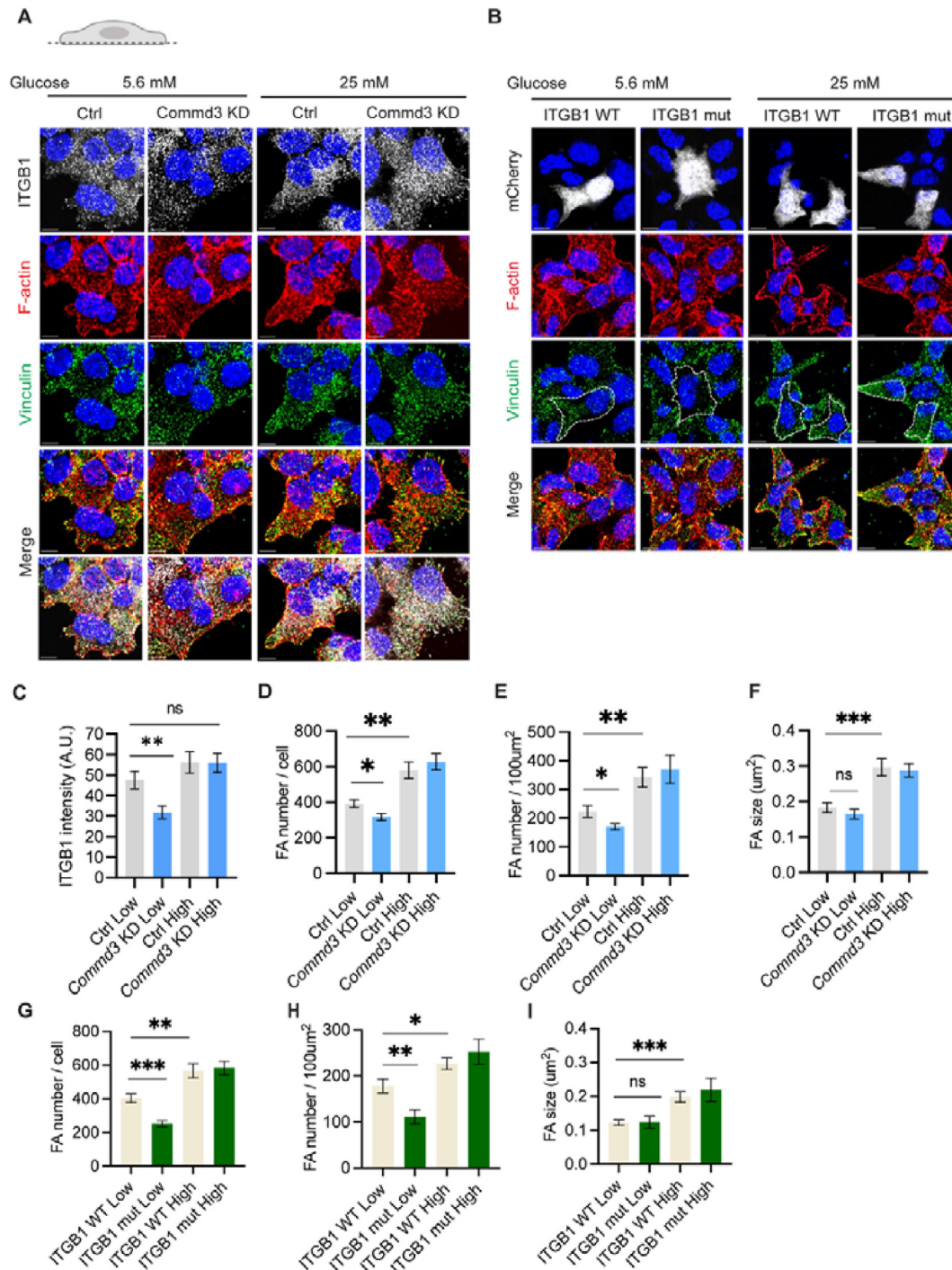


Figure 8: Defective ITGB1 recycling reduces cortical focal adhesions. (A) Representative images of ITGB1, F-actin, and Vinculin localization at basal plasma membrane of control and *Commd3* KD MIN6 cells. The cells were cultured in medium containing 5.6 mM or 25 mM glucose, fixed, stained for ITGB1 (white), F-actin (red) and Vinculin (green) and imaged with confocal microscopy. (B) Representative images of F-actin and Vinculin localization at basal plasma membrane of MIN6 cells co-expressing mCherry and WT or mutant ITGB1. The cells were transfected, cultured in medium containing 5.6 mM or 25 mM glucose, fixed, stained for F-actin (red) and Vinculin (green) and imaged with confocal microscopy. White cells indicate transfected cells. (C) Quantification of fluorescence intensity of the ITGB1 signal in control and *Commd3* KD MIN6 cells treated as in (A). (D) Quantification of focal adhesion number per cell in control and *Commd3* KD MIN6 cells treated as in (A). (E) Quantification of focal adhesion number per 100 µm² area in control and *Commd3* KD MIN6 cells treated as in (A). (F) Quantification of focal adhesion size in control and *Commd3* KD MIN6 cells treated as in (A). (G) Quantification of focal adhesion number per cell in MIN6 cells expressing WT or mutant ITGB1 treated as in (B). (H) Quantification of focal adhesion number per 100 µm² area in MIN6 cells expressing WT or mutant ITGB1 treated as in (B). (I) Quantification of focal adhesion size in MIN6 cells expressing WT or mutant ITGB1 treated as in (B). ns, no significant difference; ***P < 0.001, **P < 0.01, *P < 0.05, unpaired t test. Error bars, S.E.M.

(Figure 7A–B). However, at 25 mM glucose, the percentage of secreting cells and secretion events per cell were similar between transfected and untransfected cells (Figure 7C–D).

We further investigated whether expression of the mutant ITGB1 reduces insulin granule docking. We measured the number of docked vesicles near the basal membrane in MIN6 cells co-expressing wild type or mutant ITGB1 with mCherry. At 5.6 mM glucose, the insulin granule density near the basal membrane was decreased in MIN6 cells expressing the mutant ITGB1 compared to those expressing the wildtype ITGB1. After 1 h of glucose stimulation, however, no difference was detected in the number of insulin granules between cells expressing the mutant and wild type ITGB1 (Figure 7E–F). Taken together, these results indicate that *Commd3* KD cells have defective ITGB1 recycling at basal glucose conditions, which decreases insulin secretion and insulin granule docking.

3.7. Defective ITGB1 recycling reduces cortical focal adhesions

How defective ITGB1 recycling reduces insulin granule docking and insulin secretion is unknown. Integrin recycling regulates focal adhesion remodeling [62], which is important for GSIS [63]. Therefore, we investigated if the defective ITGB1 recycling from *Commd3* deficiency affects focal adhesions. In *Commd3* KD cells, the ITGB1 in the basal PM was significantly lower than control cells as shown by immunofluorescence (Figure 8A,C; Fig. 5). Moreover, the number of focal adhesions was significantly decreased at basal glucose level in *Commd3* KD cells compared to control cells. However, 20 min after stimulation with 25 mM glucose, the number of focal adhesions in *Commd3* KD cells became indistinguishable from control cells (Figure 8A,D–E; Figure 5A, C–D). There was no difference in the size of focal adhesions between *Commd3* KD and control cells under either basal or high glucose condition (Figure 8A,F; Figs. S5A and E). Similarly, MIN6 cells overexpressing the mutant ITGB1 had fewer focal adhesions than cells expressing the wildtype ITGB1 at basal status, but not after 20 min of 25 mM glucose stimulation (Figure 8B,G–I; Fig. S5B, F–H). These results suggest a role of diminished cortical focal adhesions in the reduced insulin granule docking and basal insulin secretion.

3.8. Reduced cortical focal adhesions diminish the assembly of ELKS complexes

Focal adhesions play an important role in polarized insulin secretion [18]. The underlying mechanism remains unclear but may relate to the ITGB1 mediated assembly of a complex consisting of Bassoon, Piccolo, RIMs, ELKS and liprins that are important for vesicle docking and exocytosis [64,65]. ITGB1 has been shown to recruit ELKS, an important scaffold of the complex, through its interaction with LL5 β and Talin-KANK1 [66,67]. ELKS is important for insulin granule docking and secretion in beta cells [21,23]. Therefore, we compared cortical ELKS in *Commd3* KD and control cells. The number of ELKS clusters was decreased and their size smaller at basal glucose compared to control cells. After 20 min high glucose stimulation, however, the number and size of ELKS clusters were indistinguishable in *Commd3* KD and control cells (Figure 9A,C–E). Similarly, in cells expressing the recycling-defective ITGB1, there were fewer and smaller ELKS clusters than in untransfected cells or cells expressing the wildtype ITGB1 at basal glucose condition. However, the difference disappeared after 20 min of high glucose stimulation (Figure 9B,F–H). These data suggest that decreased ELKS-containing complexes may be responsible for fewer docked insulin granules and decreased basal insulin secretion.

Taken together, our results demonstrated a previously unknown function of the Commander complex in basal insulin secretion. We

showed that by recycling ITGB1, Commander complex increases cortical adhesions, which enhances the assembly of the ELKS-containing complexes. The resulting increase of the number of insulin granules near the plasma membrane strengthens basal insulin secretion.

4. DISCUSSION

In the present work, we established a highly glucose responsive beta cell reporter line (MIN6-6) with multiple engineered functionalities. This line allows for CRISPR/Cas9 mutagenesis, quantification of bulk insulin secretion by a straightforward NanoLuc assay, and en masse quantification of glucose-stimulated insulin granule exocytosis in single cells. We conducted a genome-wide screen for genes affecting glucose stimulation index. Several components of the Commander complex were among the top hits of cells with increased glucose stimulation index. We demonstrated that loss of function of the Commander complex decreases basal glucose secretion with little effect on GSIS. The decreased basal insulin secretion was due, at least in part, to fewer docked insulin granules. The reduction in docked granules partially results from impaired ITGB1 recycling and the consequent reduction of cortical focal adhesions and ELKS-containing complexes.

The screen identified several genes known to regulate insulin secretion, demonstrating the validity of the assay. For example, an activating mutation in *Glud1* causes congenital hyperinsulinism [68]. Beta cells with increased *Glud1* activity have increased basal but blunted glucose-stimulated insulin secretion [69,70], consistent with an increased glucose stimulation index in cells with lower *Glud1* activity. Similarly, shRNA-mediated *Rab7* knockdown increases glucose-stimulated insulin secretion [71], consistent with the screen results. Interestingly, a number of genes encoding non-respiratory components of the mitochondria were also among the top hits in the pool of increased glucose induction index. Whether they affect basal or stimulated insulin secretion remains to be determined. Only limited genes were identified in the pool of decreased glucose induction index, however. This may be a result of the heterogeneity of the glucose responsiveness of the cells despite their clonal origin, the small shift in the distribution of the glucose induction index (Figure 1F), and the stringent selection we implemented (Figure 2B). A less stringent selection may allow identification of more genes.

The screen identified multiple components of the Commander complex, which consists of 15 subunits. *COMMD1-10*, along with *CCDC93*, can all interact with *CCDC22* to form the CCC complex. The CCC complex interacts with the retriever complex, consisting of *Vps35*, *Vps26c* and *Vps29*, to form the Commander complex [45]. Although some of the *COMMD* proteins may have preferred binding partners [72], they can all bind to each other promiscuously [44]. All 15 genes are expressed in MIN6 cells. Interestingly, knockdown of *Commd3* led to not only a reduction of protein levels of other components, but also downregulation of mRNA levels of all other genes in the complex, suggesting feedback regulation at transcription or mRNA stability (Figure 3A–B). Previously, it has been reported that hepatocyte-specific knockout of *Commd1*, *Commd6*, or *Commd9* to a lesser extent, destabilizes all Commander components [49]. Similar results have been seen in HeLa cells [48]. Our results indicate that the downregulation may be at least partially due to a decrease in mRNA levels.

We found that the increased glucose stimulation index in *Commd3* mutant cells results from lower basal insulin secretion. Both NanoLuc assay of bulk insulin secretion and FluoZin-3 assay of insulin secretion

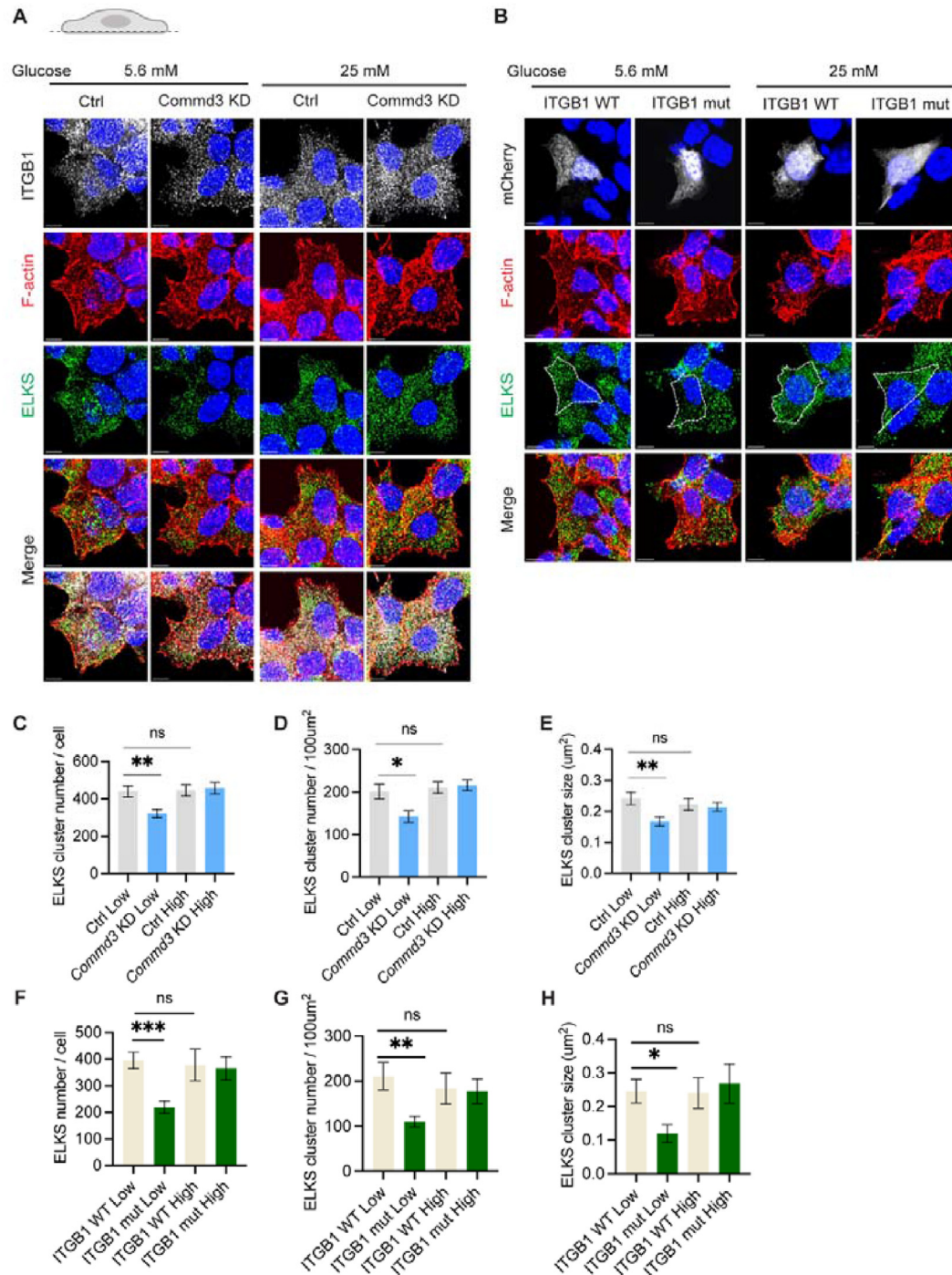


Figure 9: Reduced cortical focal adhesions diminishes the assembly of ELKS complexes. (A) Representative images of ITGB1, F-actin, and ELKS localization at basal plasma membrane of control and *Commd3* KD MIN6 cells. The cells were cultured in medium containing 5.6 mM or 25 mM glucose, fixed, stained for ITGB1 (white), F-actin (red) and ELKS (green) and imaged with confocal microscopy. (B) Representative images of F-actin and ELKS localization at basal plasma membrane of MIN6 cells co-expressing mCherry and WT or mutant ITGB1. The cells were transfected, cultured in medium containing 5.6 mM or 25 mM glucose, fixed, stained for F-actin (red) and ELKS (green) and imaged with confocal microscopy. (C) Quantification of ELKS cluster number per cell in control and *Commd3* KD MIN6 cells treated as in (A). (D) Quantification of ELKS cluster number per 100 μm^2 area in control and *Commd3* KD MIN6 cells treated as in (A). (E) Quantification of ELKS cluster size in control and *Commd3* KD MIN6 cells treated as in (A). (F) Quantification of ELKS cluster number per cell in MIN6 cells expressing WT or mutant ITGB1 treated as in (B). (G) Quantification of ELKS cluster number per 100 μm^2 area in MIN6 cells transfected with ITGB1 WT or ITGB1 mut treated as in (B). (H) Quantification of ELKS cluster size in MIN6 cells expressing WT or mutant ITGB1 treated as in (B). ns, no significant difference; *** $P < 0.001$, ** $P < 0.01$, * $P < 0.05$, unpaired t test. Error bars, S.E.M.

in single cells indicated a lower basal secretion and normal glucose-stimulated secretion in *Commd3* mutant cells (Figure 3D, Figure 4B–D). Although lower basal secretion is often a sign of maturity [73], there

was no difference in the expression of several maturity markers (Fig. S3B). Instead, we found fewer docked insulin granules at basal state in the *Commd3* mutant cells (Figure 5A–D). This contrasts with

granuphilin mutant beta cells where a decrease of docked granules slightly enhances basal insulin secretion [74]. The difference is likely due to the dual roles of granuphilin in docking and exocytosis [74,75]. COMMD3 probably does not play a direct role in either docking or exocytosis. The normal glucose-stimulated insulin secretion in *Commd3* mutant cells indicates it does not affect glucose-stimulated granule docking nor exocytosis [76].

COMMD3 has been reported to regulate ITGB1 recycling and deficiency of COMMD3 causes ITGB1 accumulation in WASH complex in HeLa cells [48]. We found in *Commd3* mutant MIN6 cells, ITGB1 accumulated in Rab4 vesicles at basal glucose (Figure 6A). This was recapitulated by expressing a recycling-deficient ITGB1 in *Commd3*-intact MIN6 cells. Expression of the recycling-deficient ITGB1 also reduced insulin secretion and insulin granule docking at basal condition but not at high glucose stimulation. ITGB1 can be recycled via different pathways depending on its partner, activation state, and cellular physiology [77]. Our results suggest that Commander-mediated recycling from Rab4-positive endosomes is the predominant pathway in beta cells at basal glucose conditions and that high glucose activates other ITGB1 recycling pathways.

The role of ITGB1 in basal insulin secretion is not clear. In two studies from the Wang lab on mice with beta cell specific loss of *Itgb1*, it was initially shown that the male mutant mice have normal fasting glucose levels but glucose intolerance, while female mutants are normal in fasting glucose and glucose tolerance [17]. In a follow up study, however, it was shown that primary islets from males, but not female, have decreased basal insulin secretion [58], similar to our results in MIN6 cells. The discrepancy may be due to the more complex regulation of insulin secretion in vivo.

Integrin mediates cell adhesion through membrane associated focal adhesions that connect to actin and the microtubule cytoskeleton [78]. As expected, impairment of ITGB1 recycling decreases membrane ITGB1 clusters and focal adhesions at basal glucose conditions (Figs. 8 and S5). Several studies have found a role for focal adhesions in GSIS [63,79,80]. Yet, how reduced focal adhesions leads to a reduction of basal insulin secretion is unknown. Genetic or pharmacological inhibition of focal adhesion kinase (FAK) reduces insulin granule docking without affecting basal insulin secretion [80,81]. It is possible that the focal adhesion effect on basal insulin secretion is FAK independent. How a reduced number of focal adhesions decreases insulin granules docking is also unknown. In the case of FAK deficiency, the diminishment of insulin granule docking is thought to be a result of impaired actin depolymerization [80,81]. In *Commd3* deficient MIN6 cells, our results suggest a decreased number and size of cortical ELKS-containing complexes as a potential mechanism. In high glucose condition, ELKS promotes exocytosis by anchoring insulin granules to the vicinity of VDCC [23]. It does not appear to occur at basal glucose conditions as no change of granule release probability was observed in *Commd3* KD cells (Figure 5E–F). Other described mechanisms of ELKS action may operate at basal glucose. The ELKS-containing complexes may promote the delivery of insulin granules by anchoring CMSCs to the focal adhesions [67], target the granules to the exocytic complexes through LL5 β -Kank1 interaction with focal adhesions [5], and/or facilitate the docking of insulin granules [22]. Although the role of ELKS in GSIS has been well established [65], its role in basal insulin secretion needs further investigations.

In summary, in a screen to identify genes that affect the glucose induction index of insulin secretion in beta cells, we identify a role for the Commander complex in enhancing basal insulin secretion. Mechanistically, we show that the Commander complex promotes docking of insulin granules at basal state. This is mediated, at least in part, by its function in

ITGB1 recycling. Defects in ITGB1 recycling reduce its membrane distribution and the number of focal adhesions. Detailed molecular mechanisms connecting focal adhesions to insulin granule docking and secretion at basal glucose conditions remain to be elucidated.

AUTHOR'S CONTRIBUTION

W.Chen conceived the project. L. Yang carried out most experiments. M.A.Fye and K. Bracy assisted FluoZin-3 assay and TIRF imaging. B. Yang and Z. Tang participated in confocal imaging and analysis. Y. Zhang assisted in bioinformatic analysis. L. Yang and W. Chen wrote and edited the manuscript. S. Haigh and B.A.Covington edited the manuscript and provided advice. I. Kevarina provided materials and advice, S. Qu and W. Chen oversaw the project.

ACKNOWLEDGMENTS

This study was supported by a Vanderbilt Discovery Grant and National Institutes of Health grants, R01DK117147 (to WC), IK was supported by the National Institutes of Health grants, R01-DK106228 and R35-GM127098. KMB was supported by a pre-doctoral fellowship from the National Institutes of Health, F31 DK122650. MAF was supported by a training grant from the National Institutes of Health, T32DK007563. BAC was supported by Molecular Endocrinology Training Program, T32DK7563-32. Confocal imaging and image analysis were performed in part through the use of the Vanderbilt Cell Imaging Shared Resource.

CONFLICT OF INTEREST

None declared.

APPENDIX A. SUPPLEMENTARY DATA

Supplementary data to this article can be found online at <https://doi.org/10.1016/j.molmet.2022.101541>.

REFERENCES

- [1] Ferrannini, E., Pilo, A., 1979. Pattern of insulin delivery after intravenous glucose injection in man and its relation to plasma glucose disappearance. *Journal of Clinical Investigation* 64(1):243–254.
- [2] Rorsman, P., Ashcroft, F.M., 2018. Pancreatic beta-cell electrical activity and insulin secretion: of mice and men. *Physiological Reviews* 98(1):117–214.
- [3] Corkey, B.E., Deeney, J.T., Merrins, M.J., 2021. What regulates basal insulin secretion and causes hyperinsulinemia? *Diabetes* 70(10):2174–2182.
- [4] Omar-Hmeadi, M., Lund, P.-E., Gandasi, N.R., Tengholm, A., Barg, S., 2020. Paracrine control of α -cell glucagon exocytosis is compromised in human type-2 diabetes. *Nature Communications* 11(1):1896.
- [5] Noordstra, I., van den Berg, C.M., Boot, F.W.J., Katrukha, E.A., Yu, K.L., Tas, R.P., et al., 2022. Organization and dynamics of the cortical complexes controlling insulin secretion in β -cells. *Journal of Cell Science* 135(3).
- [6] Gandasi, N.R., Barg, S., 2014. Contact-induced clustering of syntaxin and munc18 docks secretory granules at the exocytosis site. *Nature Communications* 5:3914.
- [7] Rorsman, P., Ashcroft, F.M., 2018. Pancreatic β -cell electrical activity and insulin secretion: of mice and men. *Physiological Reviews* 98(1):117–214.
- [8] Brun, T., Roche, E., Assimacopoulos-Jeannet, F., Corkey, B.E., Kim, K.-H., Prentki, M., 1996. Evidence for an anaplerotic/malonyl-CoA pathway in pancreatic β -cell nutrient signaling. *Diabetes* 45(2):190–198.
- [9] Stark, R., Pasquel, F., Turcu, A., Pongratz, R.L., Roden, M., Cline, G.W., et al., 2009. Phosphoenolpyruvate cycling via mitochondrial phosphoenolpyruvate

- carboxykinase links anaplerosis and mitochondrial GTP with insulin secretion. *Journal of Biological Chemistry* 284(39):26578–26590.
- [10] Ferdoussi, M., Dai, X., Jensen, M.V., Wang, R., Peterson, B.S., Huang, C., et al., 2015. Isocitrate-to-SEN1 signaling amplifies insulin secretion and rescues dysfunctional β cells. *Journal of Clinical Investigation* 125(10):3847–3860.
- [11] Gooding, Jessica R., Jensen, Mette V., Dai, X., Wenner, Brett R., Lu, D., Arumugam, R., et al., 2015. Adenylosuccinate is an insulin secretagogue derived from glucose-induced purine metabolism. *Cell Reports* 13(1):157–167.
- [12] Kalwat, M.A., Cobb, M.H., 2017. Mechanisms of the amplifying pathway of insulin secretion in the β cell. *Pharmacology & Therapeutics* 179:17–30.
- [13] Kaeser, P.S., Regehr, W.G., 2014. Molecular mechanisms for synchronous, asynchronous, and spontaneous neurotransmitter release. *Annual Review of Physiology* 76:333–363.
- [14] Huang, C., Walker, E.M., Dadi, P.K., Hu, R., Xu, Y., Zhang, W., et al., 2018. Synaptotagmin 4 regulates pancreatic β cell maturation by modulating the Ca^{2+} sensitivity of insulin secretion vesicles. *Developmental Cell* 45(3):347–361 e345.
- [15] Yasuda, T., Shibasaki, T., Minami, K., Takahashi, H., Mizoguchi, A., Uriu, Y., et al., 2010. Rim2 α determines docking and priming states in insulin granule exocytosis. *Cell Metabolism* 12(2):117–129.
- [16] Diaferia, G.R., Jimenez-Caliani, A.J., Ranjekar, P., Yang, W., Hardiman, G., Rhodes, C.J., et al., 2013. β 1 integrin is a crucial regulator of pancreatic β -cell expansion. *Development* 140(16):3360–3372.
- [17] Riopel, M., Krishnamurthy, M., Li, J., Liu, S., Leask, A., Wang, R., 2011. Conditional β 1-integrin-deficient mice display impaired pancreatic β cell function. *The Journal of Pathology* 224(1):45–55.
- [18] Gan, W.J., Do, O.H., Cottle, L., Ma, W., Kosobrodova, E., Cooper-White, J., et al., 2018. Local integrin activation in pancreatic β cells targets insulin secretion to the vasculature. *Cell Reports* 24(11):2819–2826 e2813.
- [19] Jevon, D., Deng, K., Hallahan, N., Kumar, K., Tong, J., Gan, W.J., et al., 2022. Local activation of focal adhesion kinase orchestrates the positioning of pre-synaptic scaffold proteins and Ca^{2+} signalling to control glucose-dependent insulin secretion. *Elife* 11.
- [20] Held, R.G., Kaeser, P.S., 2018. ELKS active zone proteins as multitasking scaffolds for secretion. *Open Biol* 8(2).
- [21] Ohara-Imaizumi, M., Ohtsuka, T., Matsushima, S., Akimoto, Y., Nishiwaki, C., Nakamichi, Y., et al., 2005. ELKS, a protein structurally related to the active zone-associated protein CAST, is expressed in pancreatic beta cells and functions in insulin exocytosis: interaction of ELKS with exocytotic machinery analyzed by total internal reflection fluorescence microscopy. *Molecular Biology of the Cell* 16(7):3289–3300.
- [22] Wang, S.S.H., Held, R.G., Wong, M.Y., Liu, C., Karakhanyan, A., Kaeser, P.S., 2016. Fusion competent synaptic vesicles persist upon active zone disruption and loss of vesicle docking. *Neuron* 91(4):777–791.
- [23] Ohara-Imaizumi, M., Aoyagi, K., Yamauchi, H., Yoshida, M., Mori, M.X., Hida, Y., et al., 2019. ELKS/Voltage-Dependent Ca^{2+} channel- β subunit module regulates polarized Ca^{2+} influx in pancreatic β cells. *Cell Reports* 26(5):1213–1226 e1217.
- [24] Shalem, O., Sanjana, N.E., Hartenian, E., Shi, X., Scott, D.A., Mikkelsen, T., et al., 2014. Genome-scale CRISPR-Cas9 knockout screening in human cells. *Science* 343(6166):84–87.
- [25] Doench, J.G., Fusi, N., Sullender, M., Hegde, M., Vaimberg, E.W., Donovan, K.F., et al., 2016. Optimized sgRNA design to maximize activity and minimize off-target effects of CRISPR-Cas9. *Nature Biotechnology* 34(2):184–191.
- [26] Schindelin, J., Arganda-Carreras, I., Frise, E., Kaynig, V., Longair, M., Pietzsch, T., et al., 2012. Fiji: an open-source platform for biological-image analysis. *Nature Methods* 9(7):676–682.
- [27] Trogden, K.P., Lee, J., Bracey, K.M., Ho, K.H., McKinney, H., Zhu, X., et al., 2021. Microtubules regulate pancreatic β -cell heterogeneity via spatiotemporal control of insulin secretion hot spots. *Elife* 10.
- [28] Sousa-Squiavinato, A.C.M., Rocha, M.R., Barcellos-de-Souza, P., de Souza, W.F., Morgado-Diaz, J.A., 2019. Cofilin-1 signaling mediates epithelial-mesenchymal transition by promoting actin cytoskeleton reorganization and cell-cell adhesion regulation in colorectal cancer cells. *Biochimica et Biophysica Acta (BBA) - Molecular Cell Research* 1866(3):418–429.
- [29] Steffen, A., Ladwein, M., Dimchev, G.A., Hein, A., Schwenkmezger, L., Arens, S., et al., 2013. Rac function is crucial for cell migration but is not required for spreading and focal adhesion formation. *Journal of Cell Science* 126(Pt 20):4572–4588.
- [30] Keppler, A., Gendreizig, S., Gronemeyer, T., Pick, H., Vogel, H., Johnsson, K., 2003. A general method for the covalent labeling of fusion proteins with small molecules in vivo. *Nature Biotechnology* 21(1):86–89.
- [31] Wasmeier, C., Hutton, J.C., 1996. Molecular cloning of phogrin, a protein-tyrosine phosphatase homologue localized to insulin secretory granule membranes. *Journal of Biological Chemistry* 271(30):18161–18170.
- [32] Pouli, A.E., Emmanouilidou, E., Zhao, C., Wasmeier, C., Hutton, J.C., Rutter, G.A., 1998. Secretory-granule dynamics visualized in vivo with a phogrin-green fluorescent protein chimera. *Biochemical Journal* 333(Pt 1):193–199.
- [33] Taraska Justin, W., Perrais, D., Ohara-Imaizumi, M., Nagamatsu, S., Almers, W., 2003. Secretory granules are recaptured largely intact after stimulated exocytosis in cultured endocrine cells. *Proceedings of the National Academy of Sciences* 100(4):2070–2075.
- [34] Pouli, A.E., Kennedy, H.J., Schofield, J.G., Rutter, G.A., 1998. Insulin targeting to the regulated secretory pathway after fusion with green fluorescent protein and firefly luciferase. *Biochemical Journal* 331(Pt 2):669–675.
- [35] O'Driscoll, L., Gammell, P., Clynes, M., 2004. Mechanisms associated with loss of glucose responsiveness in beta cells. *Transplantation Proceedings* 36(4):1159–1162.
- [36] Peterson, B.S., Campbell, J.E., Ilkayeva, O., Grimsrud, P.A., Hirschey, M.D., Newgard, C.B., 2018. Remodeling of the acetylproteome by SIRT3 manipulation fails to affect insulin secretion or β cell metabolism in the absence of overnutrition. *Cell Reports* 24(1):209–223.
- [37] Szymczak, A.L., Workman, C.J., Wang, Y., Vignali, K.M., Dilioglou, S., Vanin, E.F., et al., 2004. Correction of multi-gene deficiency in vivo using a single 'self-cleaving' 2A peptide-based retroviral vector. *Nature Biotechnology* 22(5):589–594.
- [38] Burns, S.M., Vetere, A., Walpita, D., Dancik, V., Khodier, C., Perez, J., et al., 2015. High-throughput luminescent reporter of insulin secretion for discovering regulators of pancreatic Beta-cell function. *Cell Metabolism* 21(1):126–137.
- [39] Hall, M.P., Unch, J., Binkowski, B.F., Valley, M.P., Butler, B.L., Wood, M.G., et al., 2012. Engineered luciferase reporter from a deep sea shrimp utilizing a novel imidazopyrazinone substrate. *ACS Chemical Biology* 7(11):1848–1857.
- [40] Miyazaki, J.-I., Araki, K., Yamato, E., Ikegami, H., Asano, T., Shibasaki, Y., et al., 1990. Establishment of a pancreatic β cell line that retains glucose-inducible insulin secretion: special reference to expression of glucose transporter isoforms. *Endocrinology* 127(1):126–132.
- [41] Cheng, K., Delghingaro-Augusto, V., Nolan, C.J., Turner, N., Hallahan, N., Andrikopoulos, S., et al., 2012. High passage MIN6 cells have impaired insulin secretion with impaired glucose and lipid oxidation. *PLoS One* 7(7):e40868.
- [42] Hart, T., Chandrashekar, M., Aregger, M., Steinhart, Z., Brown, K.R., MacLeod, G., et al., 2015. High-resolution CRISPR screens reveal fitness genes and genotype-specific cancer liabilities. *Cell* 163(6):1515–1526.
- [43] Li, W., Xu, H., Xiao, T., Cong, L., Love, M.I., Zhang, F., et al., 2014. MAGeCK enables robust identification of essential genes from genome-scale CRISPR/Cas9 knockout screens. *Genome Biology* 15(12):554.
- [44] Healy, M.D., Hospenthal, M.K., Hall, R.J., Chandra, M., Chilton, M., Tillu, V., et al., 2018. Structural insights into the architecture and membrane interactions of the conserved COMMD proteins. *Elife* 7.

- [45] Mallam, A.L., Marcotte, E.M., 2017. Systems-wide studies uncover commander, a multiprotein complex essential to human development. *Cell Syst* 4(5):483–494.
- [46] Ishigaki, K., Akiyama, M., Kanai, M., Takahashi, A., Kawakami, E., Sugishita, H., et al., 2020. Large-scale genome-wide association study in a Japanese population identifies novel susceptibility loci across different diseases. *Nature Genetics* 52(7):669–679.
- [47] Anderson, D., Cordell, H.J., Fakiola, M., Francis, R.W., Syn, G., Scaman, E.S., et al., 2015. First genome-wide association study in an Australian aboriginal population provides insights into genetic risk factors for body mass index and type 2 diabetes. *PLoS One* 10(3):e0119333.
- [48] Singla, A., Fedoseienko, A., Giridharan, S.S.P., Overlee, B.L., Lopez, A., Jia, D., et al., 2019. Endosomal PI(3)P regulation by the COMMD/CCDC22/CCDC93 (CCC) complex controls membrane protein recycling. *Nature Communications* 10(1):4271.
- [49] Fedoseienko, A., Wijers, M., Wolters, J.C., Dekker, D., Smit, M., Huijckman, N., et al., 2018. The COMMD family regulates plasma LDL levels and attenuates atherosclerosis through stabilizing the CCC complex in endosomal LDLR trafficking. *Circulation Research* 122(12):1648–1660.
- [50] Gee, K.R., Zhou, Z.L., Qian, W.J., Kennedy, R., 2002. Detection and imaging of zinc secretion from pancreatic beta-cells using a new fluorescent zinc indicator. *Journal of the American Chemical Society* 124(5):776–778.
- [51] Olofsson, C.S., Göpel, S.O., Barg, S., Galvanovskis, J., Ma, X., Salehi, A., et al., 2002. Fast insulin secretion reflects exocytosis of docked granules in mouse pancreatic B-cells. *Pflügers Archiv* 444(1–2):43–51.
- [52] Kusick, G.F., Ogunmowo, T.H., Watanabe, S., 2022. Transient docking of synaptic vesicles: implications and mechanisms. *Current Opinion in Neurobiology* 74:102535.
- [53] Obermuller, S., Lindqvist, A., Karanauskaite, J., Galvanovskis, J., Rorsman, P., Barg, S., 2005. Selective nucleotide-release from dense-core granules in insulin-secreting cells. *Journal of Cell Science* 118(Pt 18):4271–4282.
- [54] Taraska, J.W., Perrais, D., Ohara-Imaizumi, M., Nagamatsu, S., Almers, W., 2003. Secretory granules are recaptured largely intact after stimulated exocytosis in cultured endocrine cells. *Proceedings of the National Academy of Sciences of the U S A* 100(4):2070–2075.
- [55] Chen, K.E., Healy, M.D., Collins, B.M., 2019. Towards a molecular understanding of endosomal trafficking by Retromer and Retriever. *Traffic* 20(7):465–478.
- [56] Kruit, J.K., Kremer, P.H., Dai, L., Tang, R., Ruddle, P., de Haan, W., et al., 2010. Cholesterol efflux via ATP-binding cassette transporter A1 (ABCA1) and cholesterol uptake via the LDL receptor influences cholesterol-induced impairment of beta cell function in mice. *Diabetologia* 53(6):1110–1119.
- [57] Lang, T., Bruns, D., Wenzel, D., Riedel, D., Holroyd, P., Thiele, C., et al., 2001. SNAREs are concentrated in cholesterol-dependent clusters that define docking and fusion sites for exocytosis. *EMBO Journal* 20(9):2202–2213.
- [58] Peart, J., Li, J., Lee, H., Riopel, M., Feng, Z.C., Wang, R., 2017. Critical role of beta1 integrin in postnatal beta-cell function and expansion. *Oncotarget* 8(38):62939–62952.
- [59] Win, P.W., Oakie, A., Li, J., Wang, R., 2020. Beta-cell $\beta 1$ integrin deficiency affects in utero development of islet growth and vascularization. *Cell and Tissue Research* 381(1):163–175.
- [60] Isaji, T., Sato, Y., Fukuda, T., Gu, J., 2009. N-glycosylation of the I-like domain of beta1 integrin is essential for beta1 integrin expression and biological function: identification of the minimal N-glycosylation requirement for alpha5beta1. *Journal of Biological Chemistry* 284(18):12207–12216.
- [61] Juliana, C.A., Yang, J., Cannon, C.E., Good, A.L., Haemmerle, M.W., Stoffers, D.A., 2018. A PDX1-ATF transcriptional complex governs β cell survival during stress. *Molecular Metabolism* 17:39–48.
- [62] Moreno-Layseca, P., Icha, J., Hamidi, H., Ivaska, J., 2019. Integrin trafficking in cells and tissues. *Nature Cell Biology* 21(2):122–132.
- [63] Rondas, D., Tomas, A., Halban, P.A., 2011. Focal adhesion remodeling is crucial for glucose-stimulated insulin secretion and involves activation of focal adhesion kinase and paxillin. *Diabetes* 60(4):1146–1157.
- [64] Held, R.G., Liu, C., Kaeser, P.S., 2016. ELKS controls the pool of readily releasable vesicles at excitatory synapses through its N-terminal coiled-coil domains. *Elife* 5.
- [65] Ohara-Imaizumi, M., Aoyagi, K., Ohtsuka, T., 2019. Role of the active zone protein, ELKS, in insulin secretion from pancreatic β -cells. *Molecular Metabolism* 27S(Suppl):S81–S91.
- [66] Hotta, A., Kawakatsu, T., Nakatani, T., Sato, T., Matsui, C., Sukezane, T., et al., 2010. Laminin-based cell adhesion anchors microtubule plus ends to the epithelial cell basal cortex through LL5alpha/beta. *The Journal of Cell Biology* 189(5):901–917.
- [67] Bouchet, B.P., Gough, R.E., Ammon, Y.C., van de Willige, D., Post, H., Jacquemet, G., et al., 2016. Talin-KANK1 interaction controls the recruitment of cortical microtubule stabilizing complexes to focal adhesions. *Elife* 5.
- [68] Stanley, C.A., Lieu, Y.K., Hsu, B.Y., Burlina, A.B., Greenberg, C.R., Hopwood, N.J., et al., 1998. Hyperinsulinism and hyperammonemia in infants with regulatory mutations of the glutamate dehydrogenase gene. *New England Journal of Medicine* 338(19):1352–1357.
- [69] Li, C., Matter, A., Kelly, A., Petty, T.J., Najafi, H., MacMullen, C., et al., 2006. Effects of a GTP-insensitive mutation of glutamate dehydrogenase on insulin secretion in transgenic mice. *Journal of Biological Chemistry* 281(22):15064–15072.
- [70] Tanizawa, Y., Nakai, K., Sasaki, T., Anno, T., Ohta, Y., Inoue, H., et al., 2002. Unregulated elevation of glutamate dehydrogenase activity induces glutamine-stimulated insulin secretion: identification and characterization of a GLUD1 gene mutation and insulin secretion studies with MIN6 cells overexpressing the mutant glutamate dehydrogenase. *Diabetes* 51(3):712–717.
- [71] Zhou, Y., Liu, Z., Zhang, S., Zhuang, R., Liu, H., Liu, X., et al., 2020. RILP restricts insulin secretion through mediating lysosomal degradation of proinsulin. *Diabetes* 69(1):67–82.
- [72] Li, H., Koo, Y., Mao, X., Sifuentes-Dominguez, L., Morris, L.L., Jia, D., et al., 2015. Endosomal sorting of Notch receptors through COMMD9-dependent pathways modulates Notch signaling. *The Journal of Cell Biology* 211(3):605–617.
- [73] Liu, J.S., Hebrok, M., 2017. All mixed up: defining roles for β -cell subtypes in mature islets. *Genes & Development* 31(3):228–240.
- [74] Gomi, H., Mizutani, S., Kasai, K., Itohara, S., Izumi, T., 2005. Granophilin molecularly docks insulin granules to the fusion machinery. *The Journal of Cell Biology* 171(1):99–109.
- [75] Verhage, M., Sørensen, J.B., 2008. Vesicle docking in regulated exocytosis. *Traffic* 9(9):1414–1424.
- [76] Gandasi, N.R., Yin, P., Omar-Hmeadi, M., Ottosson Laakso, E., Vikman, P., Barg, S., 2018. Glucose-dependent granule docking limits insulin secretion and is decreased in human type 2 diabetes. *Cell Metabolism* 27(2):470–478 e474.
- [77] De Franceschi, N., Hamidi, H., Alanko, J., Sahgal, P., Ivaska, J., 2015. Integrin traffic - the update. *Journal of Cell Science* 128(5):839–852.
- [78] Zhen, Y., Stenmark, H., 2015. Cellular functions of Rab GTPases at a glance. *Journal of Cell Science* 128(17):3171–3176.
- [79] Arous, C., Rondas, D., Halban, P.A., 2013. Non-muscle myosin IIA is involved in focal adhesion and actin remodelling controlling glucose-stimulated insulin secretion. *Diabetologia* 56(4):792–802.
- [80] Rondas, D., Tomas, A., Soto-Ribeiro, M., Wehrle-Haller, B., Halban, P.A., 2012. Novel. Mechanistic link between focal adhesion remodeling and glucose-stimulated insulin secretion. *Journal of Biological Chemistry* 287(4):2423–2436.
- [81] Cai, E.P., Casimir, M., Schroer, S.A., Luk, C.T., Shi, S.Y., Choi, D., et al., 2012. In vivo role of focal adhesion kinase in regulating pancreatic beta-cell mass and function through insulin signaling, actin dynamics, and granule trafficking. *Diabetes* 61(7):1708–1718.